

SEAKEEPING FOR THE T-CRAFT USING LINEAR POTENTIAL AND  
NONLINEAR DYNAMIC METHODS

A Thesis

by

JOHN CHRISTIAN BANDAS

Submitted to the Office of Graduate Studies of  
Texas A&M University  
in partial fulfillment of the requirements for the degree of

MASTER OF SCIENCE

May 2012

Major Subject: Ocean Engineering

Seakeeping for the T-Craft Using Linear Potential and  
Nonlinear Dynamic Methods

Copyright 2012 John Christian Bandas

SEAKEEPING FOR THE T-CRAFT USING LINEAR POTENTIAL AND  
NONLINEAR DYNAMIC METHODS

A Thesis

by

JOHN CHRISTIAN BANDAS

Submitted to the Office of Graduate Studies of  
Texas A&M University  
in partial fulfillment of the requirements for the degree of  
MASTER OF SCIENCE

Approved by:

Chair of Committee,	Jeffrey Falzarano
Committee Members,	Moo-Hyun “Joseph” Kim
	Alan Palazzolo
Head of Department,	John Niedzwecki

May 2012

Major Subject: Ocean Engineering

## ABSTRACT

Seakeeping for the T-Craft Using Linear Potential and

Nonlinear Dynamic Methods. (May 2012)

John Christian Bandas, B.S., Texas A&M University

Chair of Advisory Committee: Dr. Jeffrey Falzarano

A system of ordinary differential equations (ODE) is constructed for an air cushion vehicle (ACV). The system is simplified to an equation for the balance of the vertical forces and the equation for the adiabatic compression of the air in the cushion. Air pressure is constantly supplied into the system, but can leak out from underneath the edges of the cushion. A series of regular waves encounters the air cushion, causing a change in volume.

Additionally, a computational analysis of the seakeeping of a Surface Effect Ship (SES) is performed using the commercial software WAMIT, which uses low-order, linear potential panel method. The model of the T-Craft consists of catamaran hulls, rigid end skirts, and the interface between the air cushion and the water surface. Beyond the six rigid body degrees of freedom of the T-Craft, additional modes are added for the motion of the interface panels. To verify the method used, the model is benchmarked using computational data for a small-scale barge model and experimental data for a T-Craft model. A comparison is performed for the T-Craft with and without its cushion.

The solution for the nonlinear time-domain system is found numerically, and the stability of the system is studied by observing bifurcations with the incoming wave amplitude as the bifurcation parameter. The system experiences a period-doubling bifurcation, from a periodic orbit, to a subharmonic orbit, to a solution with multiple periods. Further increasing the wave amplitude increases the period doubling, eventually leading to chaotic behavior.

As a result of the linear-potential simulations, significant differences are found in the seakeeping of the T-Craft when on and off the cushion. These differences are caused by the direct and indirect effects of the cushion (added aerodynamics and a decreased draft). The RAO's of the craft experience changes in amplitude and phase, which will affect the multi-body relative motions. The time-domain model shows very chaotic behaviour that is presented visually in a bifurcation diagram. These linear potential and time-domain methods illustrate the complexity and importance of modelling air-cushion effects.

## DEDICATION

To my loving parents.

## ACKNOWLEDGEMENTS

I would like to thank my committee chair, Dr. Falzarano, and my committee members, Dr. Palazzolo and Dr. Kim, for their guidance and advice throughout the course of this research.

Thanks to Kelly Cooper and the U.S. Office of Naval Research, who have supported this project through ONR Grant No. N00014-07-1-1067, and have offered many years of continued assistance.

Finally, thanks to my friends and family, especially my mother and father, for their understanding, advice, and dedicated support.

## NOMENCLATURE

$Q, \sigma$	source strength
$m$	mass of ship (15902 kg)
$A_c$	area of cushion volume (60.55 m <sup>2</sup> )
$g$	gravitational acceleration (9.81 m/s <sup>2</sup> )
$Q_{in}$	intake flowrate (0-11.2962 m <sup>3</sup> /s)
$\gamma$	polytropic gas coefficient (1.4)
$p_a$	atmospheric pressure (101.325 kPa)
$\phi$	discharge coefficient (0.7)
$\rho_a$	density of air (1.2 kg/m <sup>3</sup> )
$B_c$	breadth of cushion (3.5 m)
$a, A$	wave amplitude (m)(~.5 m lower bound, see Zhou (1980))
$\beta$	wave heading (rad)
$k$	wave number (m <sup>-1</sup> )
$L_c$	length of cushion (17.3 m)
$\omega_e$	wave frequency (rad/s)
$H$	height of sidewalls (1.22 m)
$\lambda$	wavelength (1.0061 m)



## TABLE OF CONTENTS

	Page
1. INTRODUCTION: THE DEVELOPMENT OF AIR CUSHION MODELS.....	1
2. POTENTIAL THEORY MODEL.....	9
2.1. General Potential Theory.....	9
2.1.1. Inclusion of Air Cushion Effects.....	13
2.1.2 Panelization of Ships.....	16
2.2 Potential Theory Model Simulation Benchmarks.....	21
2.2.1 Barge Computational Results.....	21
2.2.2 NSWCCD Experimental Data.....	23
2.3 Comparison of Cushion Conditions.....	25
3. NONLINEAR TIME DOMAIN SES MODEL.....	35
3.1 System and Equations Investigated.....	36
3.2 Nondimensionalization.....	42
3.3 Stability of the System.....	45
4. CONCLUSION.....	53
REFERENCES.....	56
APPENDIX A.....	58
APPENDIX B.....	59
APPENDIX C.....	64
VITA.....	87

## LIST OF FIGURES

FIGURE	Page
1 Model Barge used in Pinkster et al. (1998).....	17
2 The generic T-craft in a catamaran configuration.....	19
3 The generic T-craft on a full cushion.....	20
4 Heave RAO of the Pinkster barge in head waves.....	22
5 Pitch RAO of Pinkster barge in head waves.....	23
6 Heave RAO of T-Craft in head waves.....	24
7 Surge RAO comparison in 20° bow waves.....	26
8 Surge force comparison in 20° bow waves.....	27
9 Heave-surge added mass comparison in 20° bow waves.....	28
10 Sway RAO comparison in 20° bow waves.....	28
11 Sway force comparison in 20° bow waves.....	29
12 Sway-sway added mass comparison in 20° bow waves.....	30
13 Heave RAO comparison in 20° bow waves.....	31
14 Roll RAO comparison in 20° bow waves.....	32
15 Pitch RAO comparison in 20° bow waves.....	33
16 Yaw RAO comparison in 20° bow waves.....	34
17 Schematic of the air cushion.....	37
18 Stable spiral.....	48
19 Intersections on the surface of section for Figure 18.....	49
20 A quasiperiodic solution.....	50

21	Development of multiple-period solution.....	51
22	Sketch of bifurcation diagram.....	52
23	An air cushion ship moving in shallow water.....	55

## LIST OF TABLES

TABLE	Page
1    Dimensions of the T-Craft.....	18

## 1. INTRODUCTION: THE DEVELOPMENT OF AIR CUSHION MODELS

A surface effect ship (SES) is a type of air cushion vehicle (ACV). It consists of twin hulls, similar to a catamaran, with the air space between the hulls sealed by flexible rubber skirts at the bow and stern of the vessel, forming a cushion. Fans pump air into the cushion, increasing the pressure above atmospheric. The benefits of an SES over a conventional catamaran include improved seakeeping and less resistance when maneuvering, due to the decreased draft (submerged height) of the vessel. These advantages allow the SES to move at a higher speed using less power (Faltinsen, 1998).

The T-Craft derives its name from its ability to transform from a SES into a hovercraft with side skirts in addition to the end skirts, allowing the vessel to travel onto land. The United States Navy is interested in the T-Craft as a method of offloading supplies and equipment to coastal areas without an accessible port. The T-Craft receives these supplies from a “seabase”: a large high-speed transport vessel. The need for analyzing the motions of the T-Craft comes from the need to predict the relative motions between the T-Craft and the seabase. To predict the interactions between the two vessels, it is necessary to accurately model the T-Craft, including the aerodynamic effects of the air cushion.

In this thesis, the details of these modeling methods are adapted to the T-Craft. WAMIT is used to calculate the hydrodynamic coefficients, and the aerodynamic

---

This thesis follows the style of Ocean Engineering.

coefficients are added in to determine the response amplitude operators (RAO's). A comparison is presented with available benchmarks and with experimental data available on the T-Craft. Comparisons are made of RAO's, hydrodynamic coefficients, and forces. The T-Craft's performance is compared both on and off the cushion. These results are discussed in the context of eventually including the T-Craft model in a multi-body system with the seabase.

The dynamics of any vessel can be modeled as a spring-damper system (Zhou et al., 2000). However, the forces induced by this system are nonlinear. For example, a ship moving down into the water will be forced back up by the increased buoyancy. But this buoyancy, called the hydrostatic restoring force, will vary along the ships length due to the hull geometry and wave heights, adding non-linearity to the vessel motions. It is possible to linearize the problem by assuming small amplitude motions about a mean water level (instead of an instantaneous, varying water level due to waves) (Faltinsen, 1998). This is what is typically done for analyzing single-hulled ships. Linearization has also been done for the SES; however, linearization neglects the relationship between the waves and the air cushion system, leading to inaccuracies when modeling the vessel.

The development of dynamic models for air cushion vehicles has steadily added new complexities and characteristics of the ship-water interactions (Yun and Bliault, 2000). The initial motivation for modeling the SES was to increase its maneuverability and reach larger, stable speeds. Linear and nonlinear equations of motion solvable in the time domain were established, which include any combination of the features of air-cushion craft.

The most basic model of the SES is considering the vessel as a rigid body, including the skirts. In the case of seakeeping, the vessel has zero forward speed (without surge motions from the waves). The cushion pressure is uniform, although the pressure and volume in the cushion change due to the waves. The water level in the cushion is modeled as an adiabatic piston, and it is assumed that there is no air leakage. This piston-like motion is known as wave pumping, and has been found to significantly affect the seakeeping and maneuverability of air cushion vehicles. The wave pumping is represented in a model by adding extra degrees of freedom to the rigid body modes. Because no air is leaking, there is no damping caused by the cushion due to the cushion's energy being conserved (adiabatic and closed) (Lee and Newman, 2000). There will be added mass and stiffness for the cushion.

The major complexities associated with higher-order models were determined to be the deformation of the cushion skirts, the diffraction of the incident waves by the cushion pressure, the compressibility of the cushion air, the spatial distribution of the pressure due to nonzero speed, and the damping and added mass caused by the cushion. These features are all related to the interaction of the free surface with the ship.

One nonlinear analysis of the SES by Zhou et. al. (1980) derived two-dimensional equations of motion for both the transverse and longitudinal motions of a prototype SES in regular waves. The effects of the air cushion caused the pitch and heave (roll and heave in the transverse case) of the SES to be coupled. The nonlinear effects include buoyancy changes along the rigid hull and the air pressure in the cushion, both changing due to waves. The cushion pressure was modeled using a linearized

adiabatic gas law. The SES is moving with a forward velocity, so the cushion pressure could not be considered uniform: the center of buoyancy was shifted backwards. The calculations of the volume flow and cushion pressure depend on the leakage of air from the skirts and the characteristics of the supply fan, which both have nonlinear behavior.

Equations of motion were created for the heave, pitch, and roll, and then solved numerically over time. The time-domain data was then transformed into the frequency domain, yielding response amplitude operator (RAO) functions.

The results from the simulation demonstrated a close relationship with experimental results. The coupling of heave-pitch motion with wave pumping was demonstrated as an increase in RAOs at a certain nondimensional wave frequency. The motion of the ACV was found to be very dependent on the characteristics of the air supply fan and skirts, but the ability to control these characteristics to affect the stability of the vehicle was left to later work.

Additional nonlinear effects were studied by Sullivan et al. (1984). They identified that both air leakage and air blockage created nonlinear effects in the air cushion. The formulation is very similar to that of Zhou et al., but with additional experimental verification. Additionally, a stability diagram is constructed for the cushion, identifying limit cycles for the vertical oscillation at lower intake flowrates, and a stable frequency at higher flowrates.

Faltinsen (1998) made significant contributions to the modeling of the SES by examining the nonlinearities created by the skirt flexibility and bag leakage. The skirts were included by modeling them as sections of cables in two dimensions. Second-order



equations were created that describe the motion of these skirt sections which are combined with the typical hydrodynamic governing equations and boundary conditions of the vessel. There are two conditions created for the skirt being in and out of contact with the water surface. For both conditions, a finite element method of weighted averages is employed. When not in contact with the water, air is allowed to flow out of the cushion. The flow is considered to be quasi-steady, incompressible, and inviscid for the time and length scales being modeled (namely the length of the leakage gap and the wave lengths). When the cushion is in contact it is assumed that the connected surface is a flat line due to the large force of the water load compared to the air load. There is a possibility of “water pile-up” inside the cushion, but Faltinsen found that the error from neglecting this was small. The contact of the water leads to a different boundary condition.

This finite element model was designed to examine the vertical acceleration of the cushion in the time domain. The resonance of the air cushion is found to occur at a different frequency from the resonance of the rigid body. Faltinsen called these resonant vertical oscillation “cobblestone oscillations”. This behavior was found to be significantly dependant on the bow and stern skirts, as the leakage of air and wave impact dampens the oscillations.

The development of seakeeping models specifically for air cushion vehicles first began around the 1970’s, to study how air cushions could support large offshore structures. These models utilize potential theory and are solved in the frequency domain for the pressures and responses of the structure.

Pinkster et al. (1998) described two numerical approaches which were verified in experiments using a simple rectangular barge supported by a cushion. The motions of the structure, the free-surface, and the cushion pressure were solved either together in one system of equations or separately in multi-body equations. Linear potential theory is used in a panel method with distributed point sources. The air-cushion-water interface is modeled by a series of panels. Each panel is massless but has added mass, damping, and stiffness, and adds one degree of freedom to the system for its vertical motion. Additionally, an aerostatic stiffness term was calculated using the adiabatic gas law. These hydrodynamic and aerostatic coefficients are coupled with adjacent cushion panels.

Pinkster used potential theory to solve his problem of seakeeping of an air cushion structure based on the previous work with high speed ACV's. The same principles are used to determine the pressure inside the cushion—namely, the idea of an adiabatic piston. In this case the cushion pressure was considered uniform but time-varying since the structure is stationary. Unlike a time-domain approach, a distribution of source potential functions is used along the structure. Kinematic boundary conditions were established for the structure. The hull has a constant boundary condition while the free surface boundary is governed by a set of generalized cosines approximating the wave profile.

Pinkster discussed two ways of solving the potential functions to obtain the RAO's which he dubbed "direct" and "indirect". In the direct method, the equations of motion with all of the degrees of freedom are solved. In the indirect method, the model

is first held captive (not allowed to move) then allowed to freely float. The indirect method allowed the forces, added masses, and damping from the cushion to be separated from the contribution of the rigid body. As with Zhou, this paper demonstrated the agreement of the model with experimental results and suggested that this would be a useful tool for designing air cushion structures.

Lee and Newman (2000) analyzed a barge supported by a closed air cushion by adapting their commercial code WAMIT. The equations of motion are created for the six rigid-body motions, with the addition of extra degrees of freedom (modes) for the cushion-water interface. Where Pinkster et al. gave each cushion panel one extra vertical degree of freedom, here all the interface panels are grouped together and given a normal velocity boundary condition that is a Fourier series approximation of the surface waves, with each extra Fourier mode adding one degree of freedom to the system. Additionally, the Helmholtz equation is used to treat the interface as a membrane, which leads to an aerodynamic added mass.

In this thesis, the time-domain model of the T-Craft is simplified to the case of a rigid barge, freely floating in incident head waves. From this simplified case, the system equations are defined using the methods in (Sullivan et al., 1985; Zhou et al., 1980). The system has variables for vertical position, vertical velocity, pressure, and time, making it a four-dimensional system. The nonlinear behavior comes from the leakage of air out of the bottom of the barge cushion. The leakage is a piecewise-nonlinear damping term which only occurs for certain combinations of position and wave height. From these equations, the parameters of the intake fan system and the waves are varied to examine

the behavior of the barge. Of particular interest is the amplitude of the vertical acceleration as the parameters change.

The frequency-domain potential model also considers the T-Craft is also simplified with rigid walls, but floating in oblique waves. This ensures a response for all of the rigid body degrees of freedom. Several model tests have been done for the T-Craft's seakeeping (Bishop et al., 2011; Hughes and Silver, 2010). These model tests used two different cushion configurations: a single cushion under the vessel, and a two-cushion system separated by a skirt located amidships. From these experimental tests, this thesis examines the similarities and differences with the numerical model.

This thesis is organized to present an extension of the techniques found in these referenced works, the results of numerical simulations for the frequency- and time-domain seakeeping, and their applicability to the modeling of a coupled-body system. Section 2 presents the potential frequency domain model, benchmarks with model tests, and comparison of the T-Craft in its cushioned and uncushioned configuration. Section 3 derives the time-domain system for heave in a regular wave environment, and examines the stability of the system as a cushion pressure and wave height varies. There are three appendices that concern the time-domain model: the system of equations (Appendix A), the analytical equilibrium of the system (Appendix B), and a series of test runs for the system (Appendix C). The conclusion and references are found after Section 3.

## 2. POTENTIAL THEORY MODEL

The potential model used in this paper is implemented using the commercial software WAMIT with some additional code for the air cushion. The linear version of WAMIT is used. The term "linear" describes the way the model discretizes the surface of the ship. The potential model produces results primarily in the frequency domain, although the frequency data can be transformed to the time-domain (and vice-versa) using Fourier transforms.

### 2.1 General Potential Theory

The following is an explanation of the common boundary element method which utilizes a distribution of point sources along the mean wetted surfaces of the body (Lee and Newman, 2000; Lee and Newman, 2006).

A basic point source in infinite fluid is written as follows

$$\phi = -Q / (4\pi R) \quad (1)$$

where Q is the source strength and R is the distance from the source.

By themselves, the point sources do not describe the wetted surface of the hull. Governing equations and boundary conditions must be accounted for. The governing equation is the Laplace equation, which defines the fluid environment as incompressible and irrotational.

$$\frac{\partial^2 \Phi}{\partial x^2} + \frac{\partial^2 \Phi}{\partial y^2} + \frac{\partial^2 \Phi}{\partial z^2} = 0 \quad (2)$$

Boundary conditions include the free-surface of the fluid, the surface of the ship, and the boundary of the air cushion. The free-surface boundary describes the free surface as a composition of harmonic waves.

$$-\omega^2 \phi + g \frac{\partial \phi}{\partial z} = 0 \quad (3)$$

The waves have a circular frequency  $\omega$ .

The complex wave potential in three dimensions can be defined by

$$\phi_o = \frac{igA}{\omega} \frac{\cosh(v(z+H))}{\cosh vH} e^{-ivx \cos \beta - ivy \sin \beta} \quad (4)$$

The quantity  $v$  is found by looking at the dispersion relation

$$\frac{\omega^2}{g} = v \tanh vH \quad (5)$$

The potential  $\phi$  in this condition has complex components, and is related to the potential in the Laplace equation by the relation

$$\phi = \text{Re}(\Phi e^{i\omega t}) \quad (6)$$

The kinematic boundary condition on the ship surface assures no fluid moves through the surface by defining the normal velocity of fluid on the boundary to be equal to that of the surface:

$$\frac{\partial \phi}{\partial n} = n_3 \frac{\partial n_3}{\partial t} \quad (7)$$

Additionally, the potential should be zero at infinite depth. Another condition is that the ship may only generate waves that move away from the body (or radiate waves).

The point source that is corrected to account for these boundary conditions is known as the Green function.

$$G(x; \xi) = \frac{1}{r} + \frac{1}{r'} + \frac{2K}{\pi} \int_0^\infty dk \frac{e^{k(z+\zeta')}}{k-K} J_0(kR) \quad (8)$$

$$r^2 = (x-\xi)^2 + (y-\eta)^2 + (z-\zeta)^2 \quad (9)$$

$$r'^2 = (x-\xi)^2 + (y-\eta)^2 + (z+\zeta)^2 \quad (10)$$

This expression is for infinite water depth, with  $J_0$  as the zeroth order Bessel function. The lower-order approach to the boundary element problem allows for the components of the total potential to be separated into radiation and diffraction component. The linearization composition is written as

$$\phi = \phi_R + \phi_D \quad (11)$$

$\phi_R$  is the radiation potential caused by the ship moving harmonically and generating waves, and  $\phi_D$  is the diffraction potential created by incident waves on the ship. These potentials can be solved with the Green's function. The radiation potential is the solution for the following equation:

$$2\pi\phi(x) + \iint_{S_b} \phi(\xi) \frac{\partial G(\xi; x)}{\partial n_\xi} d\xi = \iint_{S_b} n_j G(\xi; x) d\xi \quad (12)$$

where  $S_b$  is the wetted surface of the vessel. Similarly, the diffraction potential can be solved from

$$2\pi\phi(x) + \iint_{S_b} \phi(\xi) \frac{\partial G(\xi; x)}{\partial n_\xi} d\xi = 4\pi\phi_o(x) \quad (13)$$

once the potential is obtained, the hydrodynamics of the vessel (pressures, motions, etc.) can be calculated.

For these equations it is usually necessary that they are solved numerically by defining the vessel's surface as panels. The source distribution (1) can be redefined using surface integrals and the Green's function:

$$\phi(x) = \iint_{S_b} \sigma(\xi) G(\xi; x) d\xi \quad (14)$$

Then equations (12) and (13) have their integrals discretized:

$$2\pi\phi(x) + \sum_{k=1}^N \left( \iint_{S_b} \phi(\xi) \frac{\partial G(\xi; x)}{\partial n_\xi} d\xi \right)_k = \sum_{k=1}^N \left( \iint_{S_b} n_j G(\xi; x) d\xi \right)_k \quad (15)$$

$$2\pi\phi(x) + \sum_{k=1}^N \left( \iint_{S_b} \phi(\xi) \frac{\partial G(\xi; x)}{\partial n_\xi} d\xi \right)_k = 4\pi\phi_o(x) \quad (16)$$

This discretization is what makes this panel method "low-order" : the integrals are simplified as a set of linear equations.

Once the potentials are solved, the hydrodynamic properties of the vessel can be found as well. The hydrodynamic force  $X_i$ , added mass  $a_{ij}$ , added damping  $b_{ij}$ , and added stiffness are calculated by the following integrals of the potentials over the body surface:

$$X_i = -i\omega\rho_w \int_{S_w} n_i \phi_D dS \quad (17)$$

$$a_{ij} - \left( \frac{i}{\omega} \right) b_{ij} = \rho_w \int_{S_w} n_i \phi_j dS \quad (18)$$

$$c_{ij} = \rho_w g \int_{S_w} n_i n_j dS \quad (19)$$



where  $i$  and  $j$  represent degrees of freedom of the system. These properties can then be used in a set of algebraic equations (shown in the next section) to calculate the RAO's of the vessel.

### 2.1.1 Inclusion of Air Cushion Effects

A major difference between the simulations of a single body and the T-Craft is the addition of a kinematic boundary condition for generalized modes along the water-air cushion interface (Lee and Newman, 2000). In addition to the six rigid body modes, generalized Fourier modes are added to approximate the elevation of the interface. These Fourier modes are added to the heave elevation and vertical components of the pitch and roll.

Looking at the kinematic boundary condition again,

$$\phi_{jn} = n_j \quad (20)$$

this equation can be expressed as the sum of generalized mode normal velocity

$$\phi_{jn} = n_j = u_j n_x + v_j n_y + w_j n_z \quad (21)$$

here  $j$  is the degree of freedom of the system. For the translational modes ( $j=1,2,3$ ), the kinematic boundary condition is equal to the normal of the surface, while for the rotational modes ( $j=4,5,6$ ), it is equal to the cross product of the normal vector and global coordinate vector.

$$j=1,2,3: \Phi_{jn} = N_j$$

$$j=4,5,6: \Phi_{jn} = X \times N_j \quad (22)$$

This boundary condition must be altered to account for the air cushion. On the surface of the air cushion interface (between air and water), the kinematic boundary condition can be expressed as the surface of this inner waterline.

$$j \geq 7 : N_j = -\zeta_j(x, y) \quad (23)$$

This water line has an elevation,  $\zeta$ , which can be approximated using Fourier modes in two dimensions. The Fourier modes are expressed as

$$\zeta_{mn}(x, y) = \begin{pmatrix} \cos u_m x \\ \sin u_m x \end{pmatrix} \begin{pmatrix} \cos v_n y \\ \sin v_n y \end{pmatrix} \quad (24)$$

where

$$u_m = \frac{m\pi}{2a} \quad (25)$$

$$v_n = \frac{n\pi}{2b} \quad (26)$$

and  $\zeta$  is the interface elevation,  $a$  is the cushion length, and  $b$  is the cushion width. The integers  $m$  and  $n$  are even or odd, depending on if the mode is proportional to cosine or sine, respectively. Each combination of  $m$  and  $n$  creates a new generalized mode and a new degree of freedom in addition to the rigid body degrees of freedom; the exact combination does not matter as long as the Fourier expansion is complete (converges accurately). This elevation is also the kinematic boundary condition along the interface. By using this boundary condition, the added stiffness of the cushion is embedded in the calculation of the hydrodynamic stiffness: the air cushion waterline is pressed down below the elevation of the free surface because of hydrostatic pressure.

While the water in the environment is assumed to be incompressible, the air in the cushion is compressible. To account of this, the velocity potential of the air cushion is governed by the Helmholtz equation:

$$\nabla^2 \Phi + K^2 \Phi = 0 \quad (27)$$

where  $\Phi$  is the velocity potential and  $K$  is the acoustic wave number. From the solution of this aerodynamic potential, the added-mass of the air cushion is calculated as

$$A_{ij} = \rho_a \int_{S_a} N_i \Phi_j dS \quad (28)$$

where  $i$  and  $j$  are mode indices,  $S_a$  is the interior air cushion surface (including interface),  $N$  is the unit normal vector pointing out of the cushion, and  $\rho_a$  is the density of air. It should be noted that in (3), the added-mass will be dependent on the frequency of the incoming waves, and the volume of the air cushion.

From the preceding equations, the equations of motion can be constructed:

$$\sum_{j=1}^{\infty} \xi_j \left[ -\omega^2 (a_{ij} + A_{ij} + M_{ij}) + i(\omega b_{ij}) + c_{ij} \right] = X_i \quad (29)$$

The summation represents the inclusion of the Fourier modes created by (1) in addition to the standard six degrees of freedom. The coefficients  $a_{ij}$ ,  $b_{ij}$ , and  $c_{ij}$  are the hydrodynamic added mass, damping, and stiffness matrices.  $X_i$  is the restoring force, and  $M_{ij}$  is the inertia matrix of the ship (note that for  $j > 6$ , the inertia matrix is zero). There is no damping caused by the air cushion. Damping would be included by expanding the dissipative effects of the cushion skirts, i.e., allowing air to leak from the cushion and deform the skirts. This would require some finite element modeling of the skirts structurally, which will not be done in this paper.

From (4), one can see that increasing the added mass should decrease the response if the exciting force remains the same. The relationship between the dynamic coefficients and the force will be important in a later section.

### **2.1.2 Panelization of Ships**

Three models are used in this paper: a rectangular model barge, the generic T-Craft without the cushion (a catamaran configuration), and the T-Craft on the cushion. The low-order version of WAMIT is used to simulate the models, so the accuracy of the model depends heavily on the number of panels used.

The barge, shown in Fig. 1, has 1127 panels. The dimensions of the barge are 2.5m in length, 0.78m beam, and 0.15m draft. The hull has a thickness of 0.02m on the ends and 0.06m on the sides. The static pressure in the barge is increased above the ambient air such that the water level inside the cushion is 0.05m below the still water line.

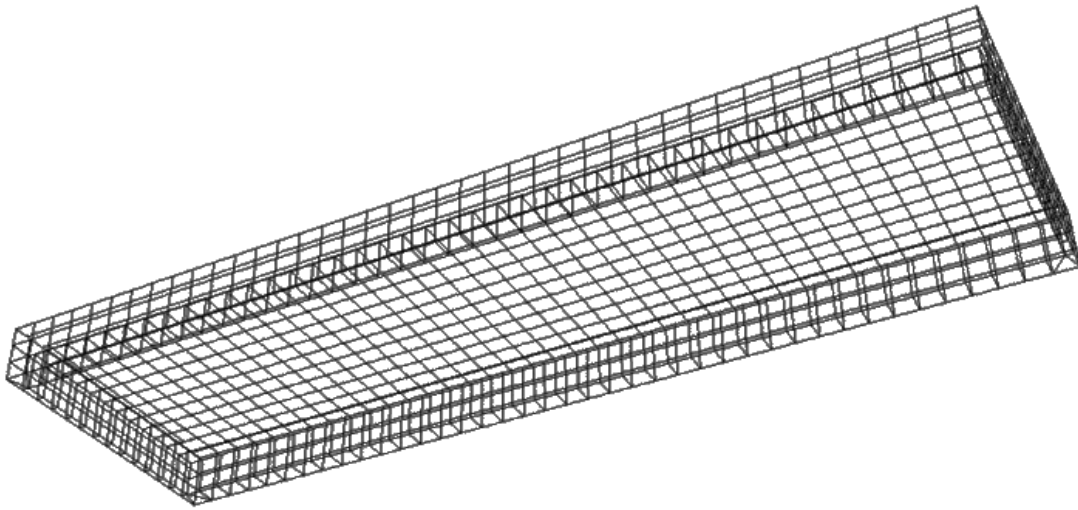


**Figure. 1.** Model Barge used in Pinkster et al. (1998)

For the barge, waterline panels were created to allow WAMIT to remove irregular frequencies from the simulation results. These panels were not necessary for the T-Craft.

The model for the generic T-Craft was provided by the Naval Surface Warfare Center Caderock Division (NSWCCD) (Hughes and Silver, 2010). This model has been used both in numerical simulations and experiments. The T-Craft has two variants: one has a single cushion, and one has two cushions created by splitting the cushion volume with a flexible plenum skirt. The dimensions of the T-Craft are shown in Table 1. Additionally, the T-Craft can be “off” the cushion, essentially becoming a catamaran. This paper models and compares the T-Craft on a single cushion and off the cushion. The wetted hull of the T-Craft off its cushion is shown in Fig. 2

**Table 1.** Dimensions of the T-Craft.

Dimension	On	Off
	Cushion	Cushion
Waterline Length (m)	67.52	75.2
Draft (m)	1.33	4.02
Cushion Width (m)	16.5	-
Cushion Length (m)	67.14	-
Cushion Height	1.3	-

The catamaran model consists of 1661 panels. The deck of the T-Craft is very close to the waterline when it is off the cushion. However, it would be very difficult to simulate the model with many panels on the waterline. Therefore, the deck is not included as part of the wetted area of the T-Craft.

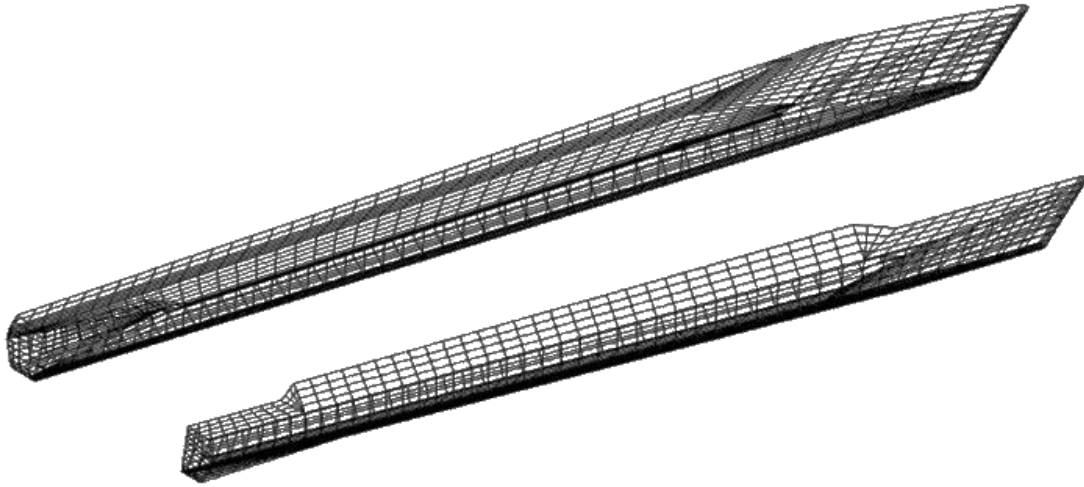


**Figure. 2.** The generic T-craft in a catamaran configuration.

To model the T-craft on its full-strength cushion, the catamaran is changed as shown in Fig. 3. The draft is decreased, and flat panels are added on the level of the inner air cushion. The skirts are modelled simply as rigid panels at the ends. The intersections between the inner hull and the air cushion create very small, sharp corners, which could cause the simulation to generate errors. Therefore, the mesh density was increased to 2232 panels.

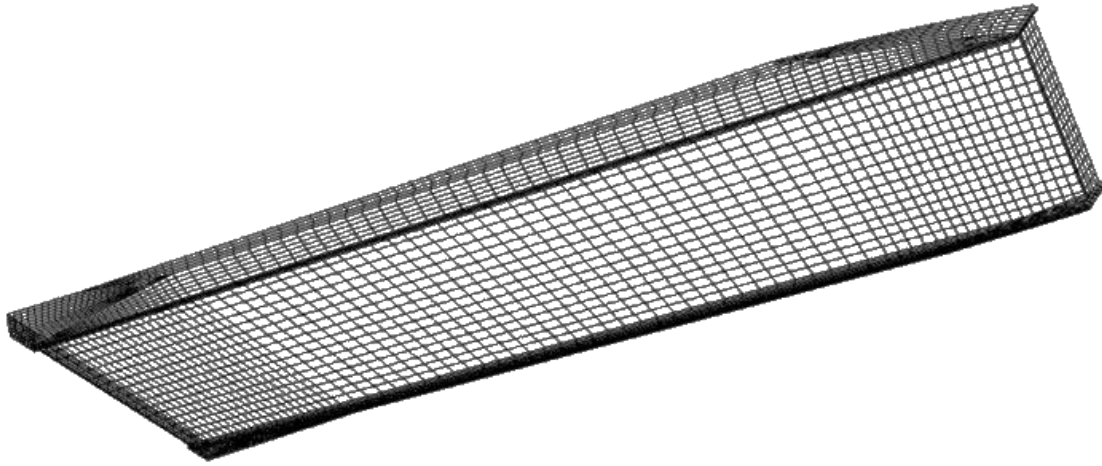


**Figure. 3.** The generic T-craft on a full cushion.

The most basic model of the SES is considering the vessel as a rigid body, including the skirts. In the case of seakeeping, the vessel is has zero forward speed. As long as the vessel is not moving, the cushion pressure is uniform. The water level in the cushion is modeled as an adiabatic piston. There will be added mass and stiffness for the cushion air.

The analysis of an air cushion vehicle using linearized potential theory is done similarly to the analysis of a single-hulled ship. The equations of motion are solved algebraically for the response by calculating the hydrodynamic coefficients and exciting forces.



## **2.2 Potential Theory Model Simulation Benchmarks**

To test the results of the simulations, two benchmarks are performed with published data. Pinkster has published forces, hydrodynamic coefficients, and response amplitude operators (RAO) for the barge. This data is generated using Pinkster's panel method, but has also been verified by Lee and Newman with the generalized modes.

Experimental data has been collected for the T-Craft by Bishop et al. (2011). Additionally, Hughes and Silver (2010) of the NSWCCD have benchmarked various seakeeping codes, including WAMIT, against the heave RAO of the experimental data. This benchmark is compared with the simulation of this paper.

### **2.2.1 Barge Computational Results**

The comparisons with Pinkster and Lee and Newman's results are shown below. In this comparison, the ship is encountering head waves. In Fig. 4, the simulated heave RAO is the solid line, and the published data is the dotted line. The data is done over a relatively large range of frequencies, but the simulation captures most of the interesting phenomena of the system. The most notable features are the humps at 6, 8, and 9 rad/s. These features are likely due to resonance with the Fourier modes of the air cushion. The simulation does not capture the feature at 9 rad/s. This could be due to a discrepancy of the number and frequency of the Fourier modes between the model and the benchmark data.

Also of note in the simulation line is a discontinuity at 3 rad/s. This was the location of an irregular frequency. An increase in the number of panels in the barge and the creation of waterline panels resulted in the data shown. There may be some small

discrepancies in the irregular frequency removal because of the presence of an inner and outer waterline.

The pitch results are shown in Fig. 5. The amplitude is the same order, but the benchmark data has its peak frequency shifted to a higher frequency. There was less data about the exact dimensions known for the model barge than for the T-Craft experimental model: adjusting the mass matrix--particularly the moments of inertia of the barge will shift the peak to a higher or lower frequency. It should be noted that the benchmark was generated using a higher order panel method.

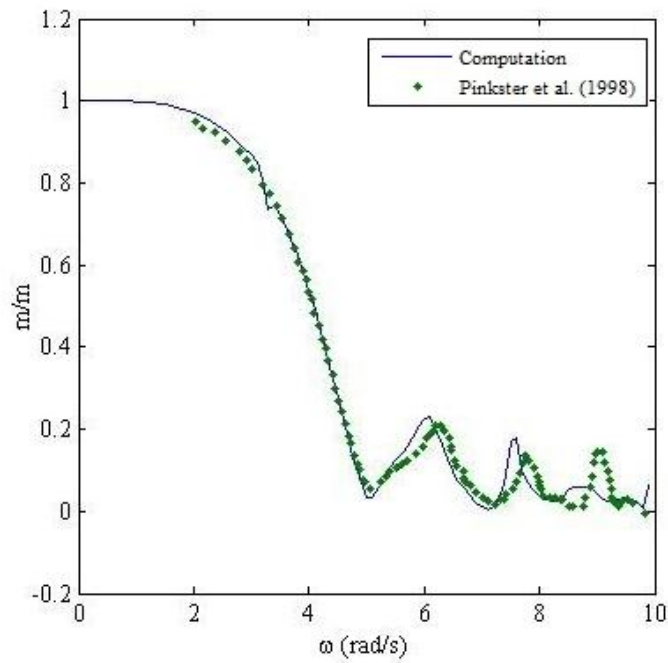


**Figure. 4.** Heave RAO of the Pinkster barge in head waves.

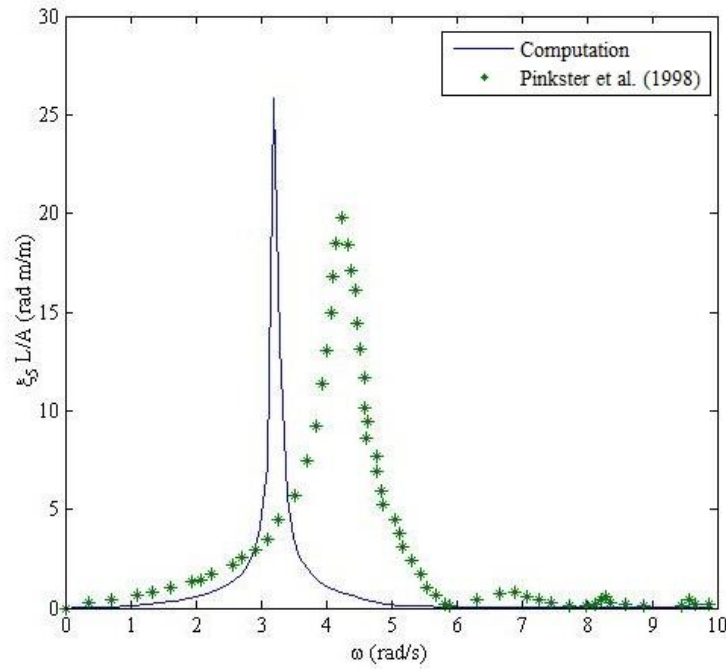


**Figure. 5.** Pitch RAO of Pinkster barge in head waves.

### 2.2.2 NSWCCD Experimental Data

For the T-Craft, Hughes and Silver (2010) used the linear, first order version of WAMIT to generate the RAO of the T-Craft. The simulation and experiment were conducted at relatively low frequencies compared to Pinkster. The wave frequencies are likely more realistic for what the T-Craft will encounter in seakeeping. Higher frequencies do become important in maneuvering.

The comparison of the simulated T-Craft, Hughes simulation, and experimental data in head waves is shown in Fig. 6. This paper's results are the solid line, Hughes data is the dashed line, and the experimental data is the dotted line. It is apparent that linear simulation is missing some behaviour found in the real T-Craft, although the agreement

between the two linear computation results is good. A very significant nonlinearity would arise from the dissipative effects of the deforming air cushion skirts. Wave impacts on the skirt, interactions of the cushion air with the fan supply system, and air leakage under the seal are some major features of the T-Craft that are not included in a linear potential source code (see Yun and Bliault, 2000). There may also be some discrepancies created by nondimensionalizing the results of linear and nonlinear data.

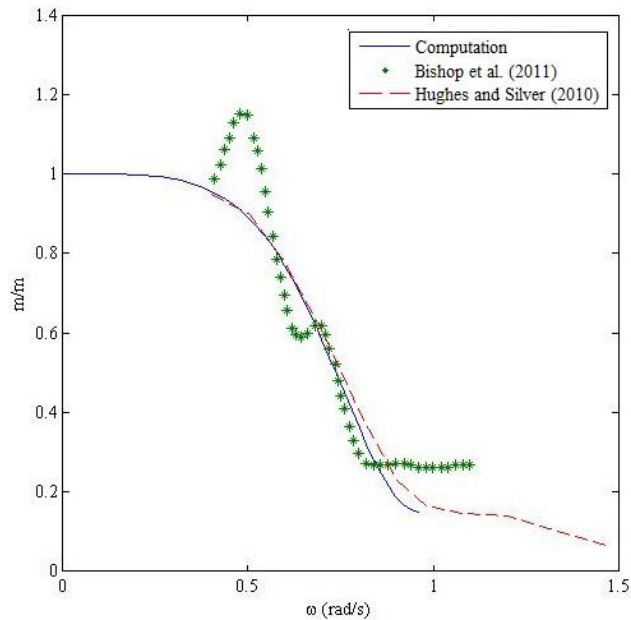


**Figure. 6.** Heave RAO of T-Craft in head waves.

Another explanation could be effects from the division of the cushion into two sections by the plenum skirt in the middle. In this case, the generalized modes would be

implemented differently for each sub-cushion, leading to an increase in total modes. This case was run in WAMIT, however, and nothing resembling the shape of the model data was found.

### **2.3 Comparison of Cushion Conditions**

To see what advantages the T-Craft has in seakeeping with its extra modes, it is desirable to know the difference gained between the T-craft on and off the cushion. The following section compares the RAO for the two cushion states. The frequency range was restricted from 0 to 2 rad/s because any higher frequency features were insignificantly small.

For all of the following figures, the solid line represents the T-Craft on its cushion and the dotted line is the T-Craft without its cushion. The ships are encountering waves at a  $20^\circ$  heading.

Some interesting behaviour appears when comparing the response of the T-Craft on and off the cushion. The surge RAO is shown in Fig. 7. Surprisingly, the surge for the T-Craft is similar both on and off the cushion. This can be explained by looking at the values of the added masses, stiffnesses, and forces. While the draft has decreased, the frontal area is roughly the same due to the inclusion of the skirts. This area is redistributed to be closer to the free surface, where there are higher pressures acting on the ship. Therefore the surge exciting force on the T-Craft is greater on the cushion compared to off the cushion for high frequencies, and smaller at low frequencies. The surge exciting force is shown in Fig. 8. The fluctuations seen in the curves are similar in phase. Although the force is higher, the some of the hydrodynamic added masses are

smaller. The heave-surge added mass is shown in Fig. 9; the decrease in draft has decreased the added masses as well as the forces. It is interesting to note that the added masses are negative across the range of frequencies. The variations in force mitigate the variations of the hydrodynamic coefficients and result in similar responses.

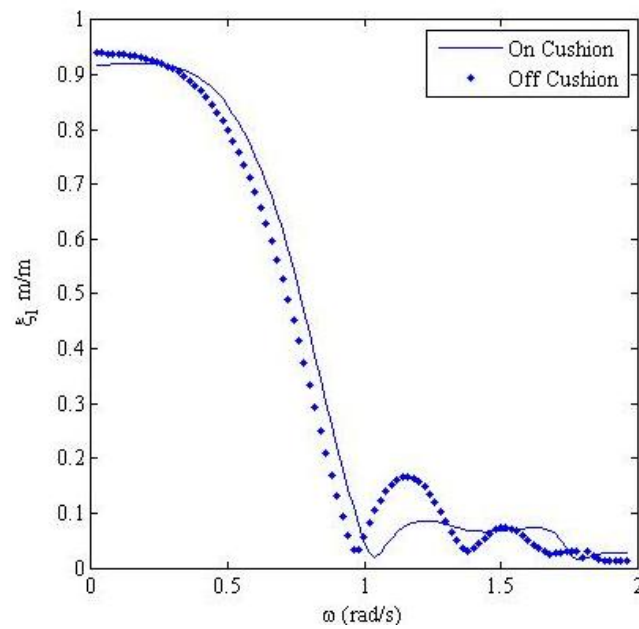


**Figure. 7** Surge RAO comparison in 20° bow waves.

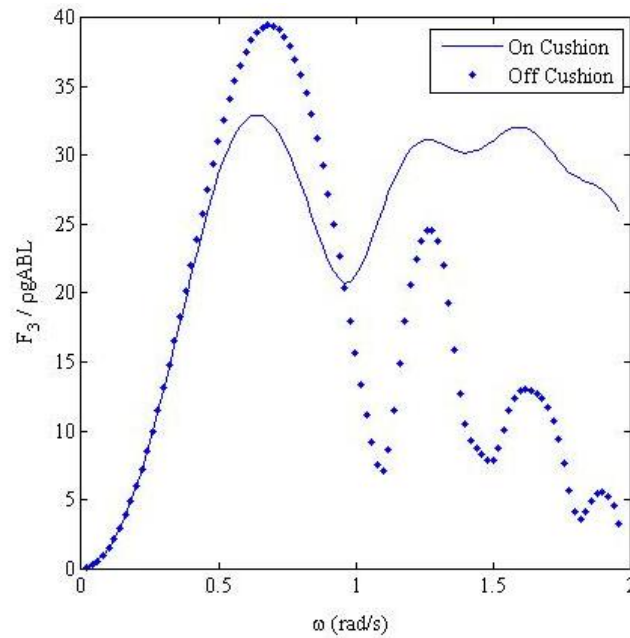


**Figure. 8** Surge force comparison in 20° bow waves.

The comparison of sway RAO's, shown in Fig. 10 supports this idea of the sensitivity of the response to change in projected area. The sway of the T-Craft is larger on the cushion. However, as shown in Fig. 11, the exciting force is actually greater when the T-Craft is off of the cushion (note there is some asymptotic behavior at higher frequencies that should be is a discrepancy in the computation). This greater force comes from the increased draft and projected area. The larger force for the catamaran seems to contradict its lesser sway response.

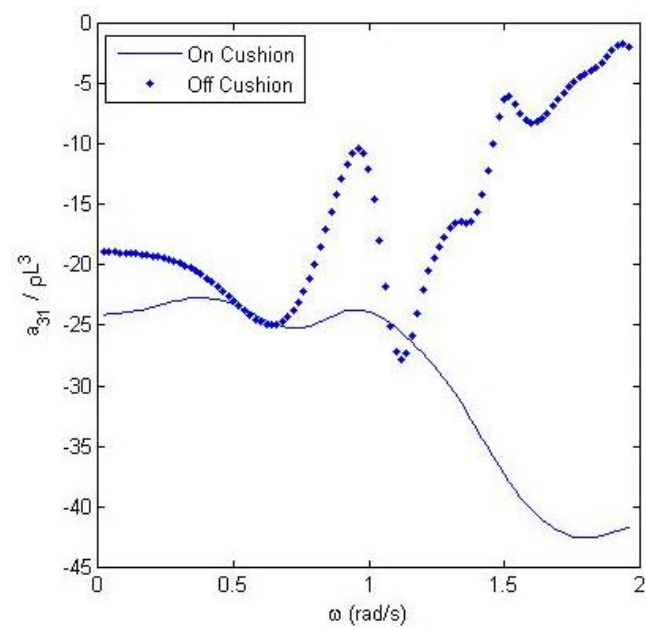


**Figure. 9** Heave-surge added mass comparison in 20° bow waves.

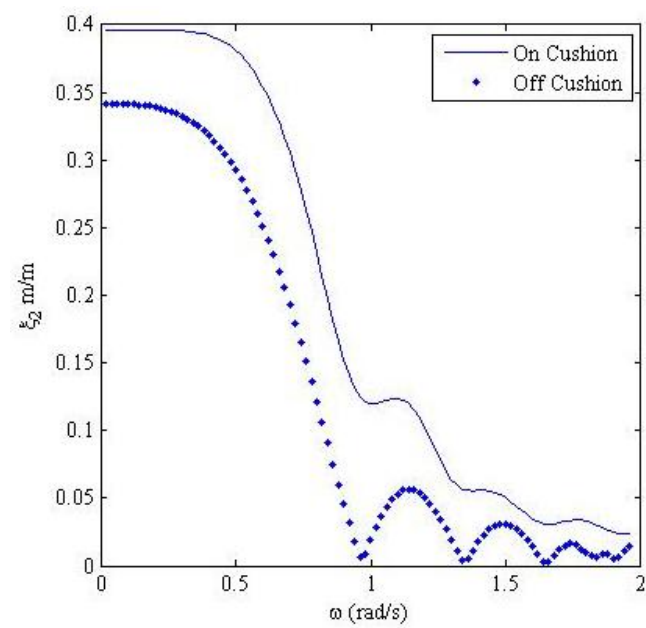


**Figure. 10.** Sway RAO comparison in 20° bow waves.



However, a change in the added mass matrices again affects the response of the ship. Smaller added masses will increase the RAO calculated as well as larger forces. Some of the sway added masses are very small or even negative for the T-Craft on its cushion. One of these coefficients, the sway-roll added mass, is compared in Fig. 12. When on the cushion, an added mass is generated that is smaller over the entire range of frequencies. The difference comes from the integration of (3), since the T-Craft has the added boundary conditions of (1). When rolling, instead of just accelerating the water displaced around a rigid body, the water volume is acting with the cushion. As a result, the contributions of the smaller added masses with the higher force creates a RAO that is higher for the T-Craft on its cushion.

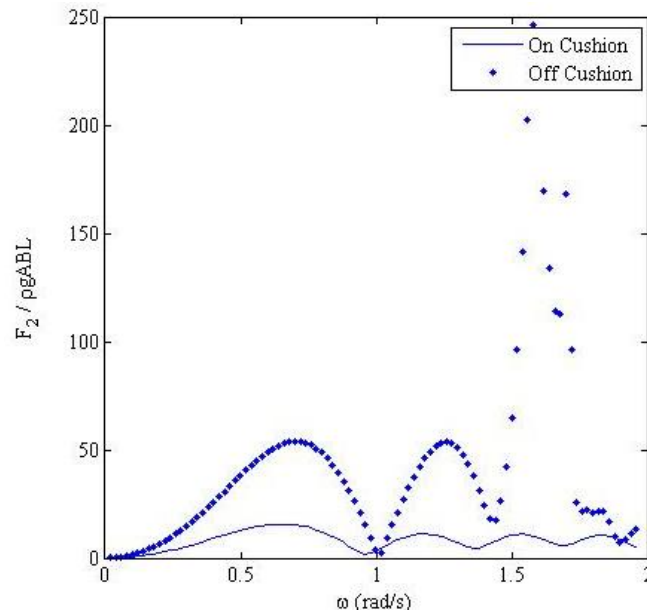


**Figure. 11** Sway force comparison in 20° bow waves.

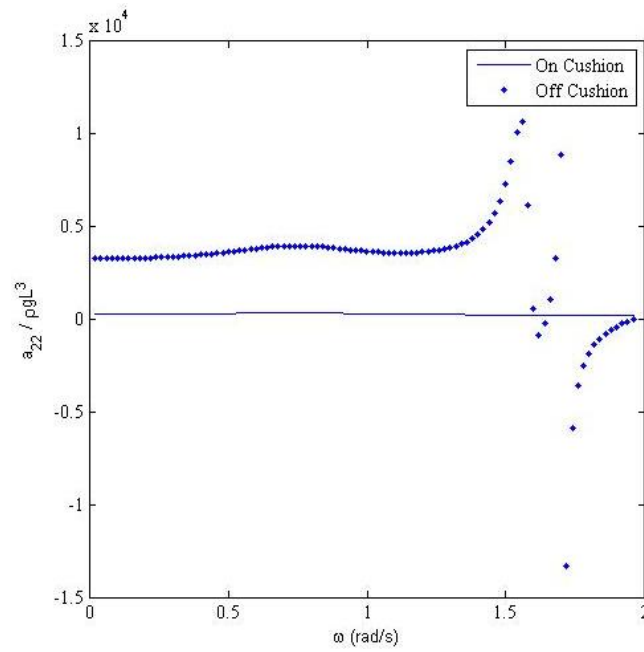


**Figure. 12.** Sway-sway added mass comparison in 20° bow waves.

The heave RAO shown in Fig. 13 is very similar both on and off the cushion. The very low frequencies dominated by hydrostatic effects are virtually unchanged, and at the higher frequencies the T-Craft cushion has a response that fluctuates less. This is accounted for by the pressure of the air cushion replacing lost buoyancy due to decreased draft, and the very small change in the projected area of the T-Craft from the bottom.

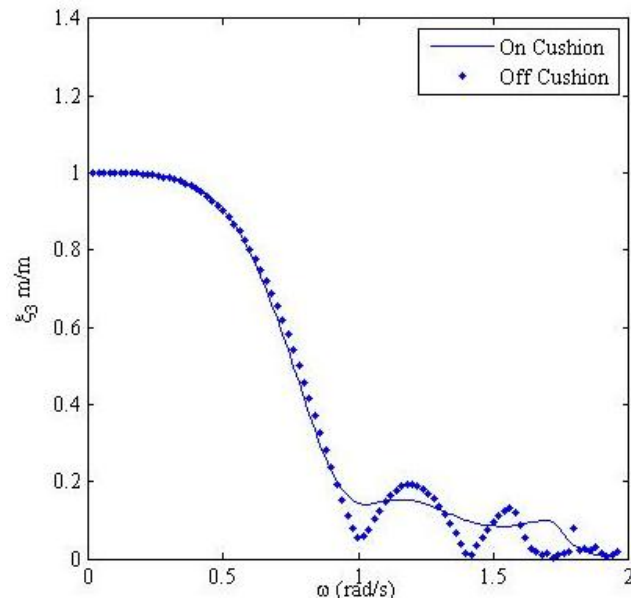


**Figure. 13.** Heave RAO comparison in 20° bow waves.

The roll RAO, shown in Fig. 14, is relatively small for both cases. However, there is an increase in the roll behaviour when the T-Craft is on the cushion. The decreased draft and the addition of air pressure decreases the righting of the T-Craft.

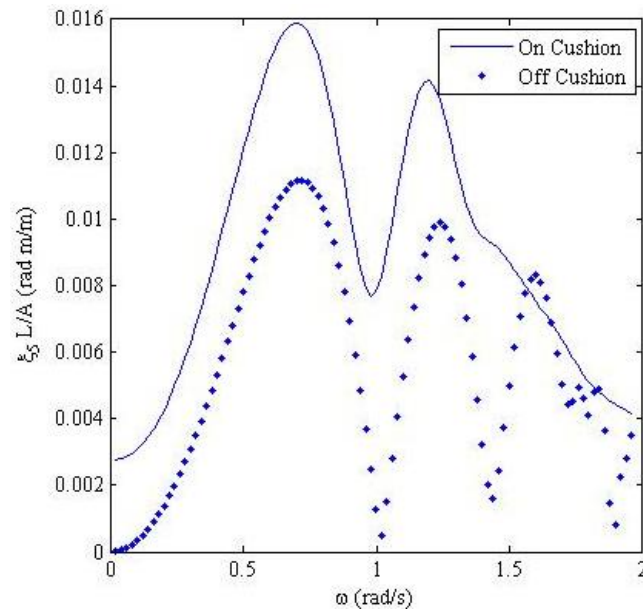


**Figure. 14.** Roll RAO comparison in 20° bow waves.

The pitch RAO is also relatively small. In Fig. 15, the response on the cushion is lower. As with the surge, this similarity could be due to the presence of the rigid skirts, whose faces are at an angle from the vertical plane. The forces on these skirt panels cause some additional moment in the longitudinal plane. The T-Craft is very long compared to its width, which is why the difference in pitch is much smaller than the difference in roll.

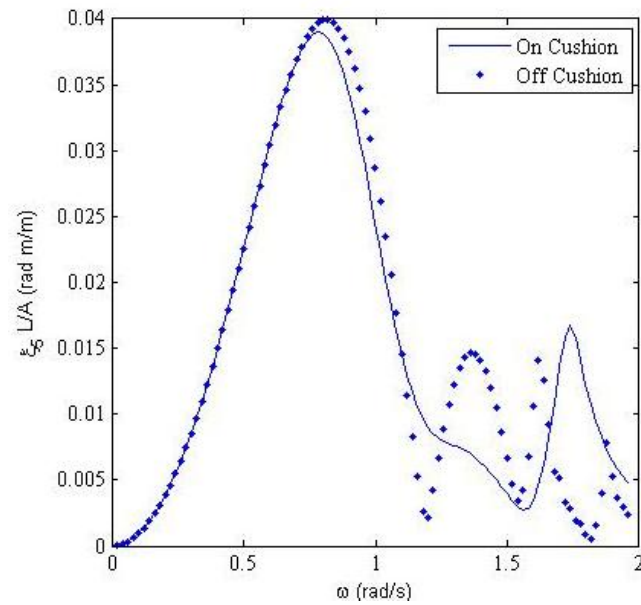


**Figure. 15.** Pitch RAO comparison in 20° bow waves.

The yaw RAO is shown in Fig. 16. The responses are once again small, although the yaw of the T-Craft on its cushion is significantly larger. The decreased draft that allows the T-Craft to have low drag also gives it higher motions in the rotational degrees of freedom. An extra moment is exerted by the skirts.

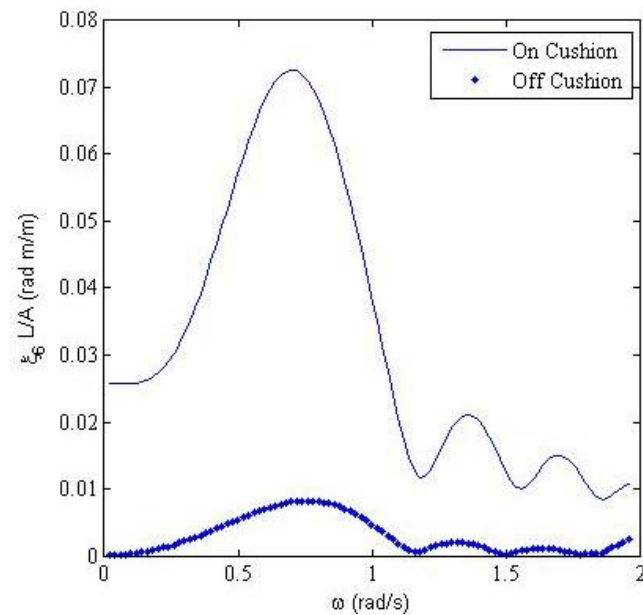


**Figure. 16.** Yaw RAO comparison in 20° bow waves.

It is apparent that the skirts and cushion have an important effect on the RAOs of the T-Craft. The assumption of rigid skirts is necessary for the linear panel method, but creates large flat areas for the exciting force to act on. Allowing the cushion skirts to deform would add damping to the system. It could be possible to add some empirical damping from the skirts, but there is no data readily available concerning this. In addition to the deformation of the skirts, the air cushion supply has some energy loss. The equations of the fan performance could be coupled to the equations of motion to account for this.

### 3. NONLINEAR TIME DOMAIN SES MODEL

To fully express the behavior of the SES, several papers outline the nonlinear analysis of the T-Craft. Zhou et. al. (1980) derived two-dimensional equations of motion for both the transverse and longitudinal motions of the SES. These models include the air leakage.

Not all of the nonlinear effects of the SES will be considered. The cushion skirts will be considered as rigid. The deformation of the bow and stern skirts due to wave impact loads contributes to large accelerations in the vertical direction when the wave encounter frequency is high (the so-called “cobblestone effect”). But this research concerns the SES at zero-forward speed, so it is unlikely that the vessel will encounter such high frequency waves. Another assumption from the zero-speed condition is that the pressure in the cushion will be uniform.

For the equations of motion, the heave, roll, and pitch are coupled, but the sway and surge are not. For the transverse direction, the transverse equation of motion is:

$$\begin{bmatrix} w/g & 0 \\ 0 & I_\theta \end{bmatrix} \begin{bmatrix} \ddot{\zeta}_g \\ \ddot{\theta} \end{bmatrix} = \begin{bmatrix} F_c \\ M_c \end{bmatrix} + \begin{bmatrix} F_s \\ M_s \end{bmatrix} + \begin{bmatrix} F_{swR} \\ M_{swR} \end{bmatrix} + \begin{bmatrix} F_{swL} \\ M_{swL} \end{bmatrix} + \begin{bmatrix} 0 \\ M_{jjR,L} \end{bmatrix} + \begin{bmatrix} W \\ 0 \end{bmatrix} \quad (30)$$

Here the heave and roll are coupled. In the longitudinal direction, the heave and pitch is coupled into the following equations of motions:

$$\begin{bmatrix} w/g & 0 \\ 0 & I_\psi \end{bmatrix} \begin{bmatrix} \ddot{\zeta}_g \\ \ddot{\psi} \end{bmatrix} = \begin{bmatrix} F_c \\ M_c \end{bmatrix} + \begin{bmatrix} F_s \\ M_s \end{bmatrix} + \begin{bmatrix} F_b \\ M_b \end{bmatrix} + \begin{bmatrix} W \\ M_0 \end{bmatrix} \quad (31)$$

For these equations, the quantities are defined as follows:  $\zeta$  is the heave,  $\psi$  is the pitch, and  $\theta$  is the roll;  $F$  and  $M$  denotes force and moment, respectively; the subscript  $c$  denotes cushion pressure contributions,  $s$  denotes skirt forces,  $swL/swR$  denote port and starboard sidewall forces,  $jj$  denotes air jet forces from the cushion gap,  $b$  denotes buoyancy, and  $0$  denotes thrust and drag; and  $w$  is the weight.

These equations are part of an iterative process: solving for the heave, roll, and pitch, as well as the velocities and accelerations, the geometric and wave parameters can be refined to recalculate the forces and moments (Zhou et al., 1980; Yun and Bliault, 2000). This leads to a numerical solution of the motions in the frequency domain.

### 3.1 System and Equations Investigated

The model used to investigate the vertical motion of the cushion is shown in Fig. 17. The geometry of the barge is taken to be rectangular, with height  $H$ , length  $L_c$ , and width  $B_c$ . The center of gravity is assumed to be in the middle of the cushion (this is also where the origin of our global coordinate system is). The walls (which represent the skirts of the air cushion) are considered to be rigid. A single duct with a known constant flowrate  $Q_{in}$  as a function of duct pressure  $p_f$  supplies air for the system. Regular incident waves move along the longitudinal axis of the cushion with amplitude  $a$  and frequency  $\omega$ . The wave height is described by the following equation:

$$\eta = a \sin(\omega t - kx) \quad (32)$$

where  $\eta$  is the instantaneous wave elevation and  $x$  is the longitudinal position of the wave with respect to the global origin  $o$ . It is assumed that the system is floating in





The air cushion pressure supports most of the weight of the ship (Faltinsen, 2005). Therefore, the effect of buoyancy can be neglected. The pressure and volume of the cushion will change over time, but for any instant the pressure can assumed to be uniform throughout the volume. This, combined with neglecting buoyancy, eliminates any pitch or roll moment from the vessel. No sway or surge motion is considered, meaning that the vessel is only moving in the heave direction.

For this system, the dependent variables are the elevation of the barge from the mean water level (MWL) to the top of the cushion  $z$  and the cushion pressure  $p_c$ . Newton's law is used to describe the forces on the cushion. The two forces are the weight and the force of the cushion pressure:

$$m \frac{d^2 z}{dt^2} = A_c p_c - mg \quad (32)$$

Here  $A_c$  is the cushion sectional area and  $m$  is the mass of the ship. Mass conservation must be observed inside the cushion volume. The equation for mass conservation is expressed as

$$Q_{in} = Q_o + Q_v + Q_p \quad (33)$$

$Q_p$  is the change in volume due to the compression of the cushion air. In this model, the pressure changes are assumed to be isentropic, which can expressed by the relation  $\frac{p}{\rho^\gamma} = \text{constant}$ , where  $\rho$  is the gas density and  $\gamma$  is a specific heat ratio. One can show that this relation can be rearranged to express the flowrate due to compression as

$$Q_p = \frac{V_c}{\gamma(p_c + p_a)} \frac{dp_c}{dt} \quad (34)$$

The volume of the cushion  $V_c$  is found by integrating the height of the cushion above the instantaneous water level and multiplying by the area of the cushion (Faltinsen, 2005):

$$V_c = zA_c - \frac{2B_c a}{k} \sin\left(\frac{kL_c}{2}\right) \sin(\omega t) \quad (35)$$

The flowrate due to volume change  $Q_v$  is simply the derivative of the expression for volume:

$$Q_v = \dot{V}_c = \frac{dz}{dt} A_c - \frac{2B_c a \omega}{k} \sin\left(\frac{kL_c}{2}\right) \cos(\omega t) \quad (36)$$

$Q_o$  represents the flowrate due to air leaking from under the walls of the cushion. This flowrate is derived from Bernoulli's expression for flow through an orifice

$$Q_o = \phi \sqrt{\frac{2}{\rho_a} |p_c|} * \text{sign}(p_c) (A_{ends} + A_{side}) \quad (37)$$

where  $\phi$  is a coefficient for the orifice flow. The absolute value and sign function of  $p_c$  allows for the possibility of flow reversal (a lower cushion pressure than atmospheric causes flow into the cushion).  $A_{ends}$  and  $A_{side}$  are the leakage areas for the edges of the cushion. The leakage is caused by a gap between the instantaneous water level and the bottom of the cushion wall. The area of leakage on the ends are expressed by

$$A_{ends} = B_c \left( \frac{z - H - a \sin\left(\omega t + \frac{kL_c}{2}\right) + \left| z - H - a \sin\left(\omega t + \frac{kL_c}{2}\right) \right|}{2} + \frac{z - H - a \sin\left(\omega t - \frac{kL_c}{2}\right) + \left| z - H - a \sin\left(\omega t - \frac{kL_c}{2}\right) \right|}{2} \right) \quad (38)$$

Notice the value of  $x$  for the front end is  $\frac{kL_c}{2}$  and for the back end is  $-\frac{kL_c}{2}$ . The absolute values allow for flow-shutoff: if the leakage gap, denoted by  $z - H - a \sin(\omega_e t + kx)$ , is equal to or less than zero, there is no leakage flow from that end. The area of leakage on the side is similar to  $A_{ends}$ , with the exception that the instantaneous water level varies along the sides of the cushion. Therefore, the leakage gap must be integrated along the length of the cushion:

$$A_{side} = \int_{-\frac{L_c}{2}}^{\frac{L_c}{2}} H - z + a \sin(\omega t - kx) + \left| H - z + a \sin(\omega t - kx) \right| dx \quad (39)$$

Due to the area terms  $Q_0$  is explicitly time-dependent and strongly nonlinear.

Looking at the mass conservation equation and  $Q_p$ , one can see that the equation can be rearranged as

$$Q_p = Q_{in} - Q_o - Q_v$$

$$\frac{V_c}{\gamma(p_c + p_a)} \frac{dp_c}{dt} = Q_{in} - \varphi \sqrt{\frac{2}{\rho_a}} |p_c|^* \text{sign}(p_c) (A_{ends} + A_{side}) - \frac{dz}{dt} A_c - \beta \cos(\omega t) \quad (40)$$

where

$$\beta = \frac{2B_c a \omega}{k} \sin\left(\frac{kL_c}{2}\right)$$

Combining (40) with (32) and setting a variable

$$\frac{dz}{dt} = y \quad (41)$$

There are three first-order ordinary differential equations that describe the system

(32, 40, 41):

$$m \frac{d^2 z}{dt^2} = A_c p_c - mg \quad (32)$$

$$\frac{V_c}{\gamma(p_c + p_a)} \frac{dp_c}{dt} = Q_{in} - \varphi \sqrt{\frac{2}{\rho_a}} |p_c| * \text{sign}(p_c) (A_{ends} + A_{side}) - \frac{dz}{dt} A_c - \beta \cos(\omega t) \quad (40)$$

$$A_{ends} = B_c \left( \frac{z - H - a \sin\left(\omega t + \frac{kL_c}{2}\right) + \left| z - H - a \sin\left(\omega t + \frac{kL_c}{2}\right) \right|}{2} + \frac{z - H - a \sin\left(\omega t - \frac{kL_c}{2}\right) + \left| z - H - a \sin\left(\omega t - \frac{kL_c}{2}\right) \right|}{2} \right)$$

$$A_{side} = \int_{-\frac{L_c}{2}}^{\frac{L_c}{2}} H - z + a \sin(\omega t - kx) + \left| H - z + a \sin(\omega t - kx) \right| dx$$

$$\alpha = \varphi \sqrt{\frac{2}{\rho_a} |p_c|} * \text{sign}(p_c)$$

$$\beta = \frac{2B_c a \omega}{k} \sin\left(\frac{kL_c}{2}\right)$$

$$\frac{dz}{dt} = y \tag{41}$$

This system is strongly nonlinear, nonautonomous, and four dimensional ( $z$ ,  $p_c$ ,  $y$ , and  $t$ ). The assumptions of rigid walls and constant intake remove some of the nonlinear complexity from the system. The remaining nonlinear effects are the variable outflow and flow-shutoff due to the relative positions of the skirt/walls and water surface. These remaining nonlinearities are universal for all air cushion systems and worth investigating (Pinkster et al., 1998). For a more comprehensive system, the effect of cushion pressure on the duct and fan could be considered, using the characteristic equations of the fan (Yun and Bliault., 2000). Additionally, the effects of cushion deformation and wave impact forces are discussed in (Faltinsen and Ulstein, 1998).

### 3.2 Nondimensionalization

Nondimensional scales are defined for the cushion pressure, vessel elevation and time. The purpose of the nondimensionalization is to standardize the system for any arbitrary selection of scales, and to compare the numerical order of each variable and

parameter. By comparing the nondimensional coefficients some general observations about the system can be made.

The first step is to substitute the system variables as the product of a nondimensional variable and a dimensional coefficient. These are shown below.

$$p_c = Pq ; z = Zx ; t = T\tau ; y = \frac{Z}{T} \frac{dx}{d\tau} \quad (42)$$

To find the values of P, Z, and T, (16) is substituted into the system of equations, make the leading order term equal to one, and then solve for the dimensional coefficient. Substituting into (6) yields:

$$m \frac{Z d^2 x}{T^2 d\tau^2} = A_c P q - mg \quad (43)$$

The equation is divided by  $\frac{mZ}{T^2}$ , and the first term is set equal to one.

$$\frac{A_c T^2 P}{Zm} = 1 \quad (44)$$

Solving for  $T^2$ ,

$$T^2 = \frac{mZ}{A_c P} \quad (45)$$

This quantity is similar to the inverse of the natural frequency of a freely vibrating system,  $\omega_n = \sqrt{\frac{k}{m}}$ , where k is a stiffness. It is also worth noting that our coefficient for time has nothing to do with the frequency of the incoming waves. As will be shown in the section examining the stability, the time scale of (45) and the time scale of the incoming waves will have interesting interactions. Unfortunately, the time

scale is a function of  $Z$  and  $P$ , so these two quantities must be defined to fully define (45).

We will find the values of  $Z$  and  $P$  by nondimensionalizing the equation for pressure equilibrium. The nondimensionalization of (40) is much more complicated, not only due to the sheer length of the equation but also how it is structured. The substitutions are made on the left hand side term:

$$\frac{V_c}{\gamma(p_c + p_a)} \frac{dp_c}{dt} = \frac{V_c}{\gamma(p_c + p_a)} \frac{Pd\tau}{Td\tau} \quad (46)$$

Using (35) to substitute into  $V_c$ , the left hand term will be

$$\frac{P(ZxA_c - h \sin(\omega_e T\tau))}{T\gamma(Pq + p_a)} \frac{dq}{dt} \quad (47)$$

where

$$h = \frac{2B_c a}{k} \sin\left(\frac{kL_c}{2}\right) \quad (48)$$

It would be very difficult to separate the nondimensional variables  $x$  and  $q$ , since they are in complicated expressions in both the numerator and denominator. To find the dimensional coefficient  $Z$ , the numerator term of (47) is examined. The  $ZxA_c$  term has the highest order; dividing yields

$$\frac{h}{A_c Z} = 1 \quad (49)$$

or

$$Z = \frac{h}{A_c} \quad (50)$$



Thus  $Z$  is defined as the ratio of the magnitude of the volume displaced by the incoming waves and the area of the air cushion.

Dividing (47) by  $Q_{in}$  on the right hand side of (40),

$$\frac{Tp_a Q_{in}}{hP} = 1 \quad (51)$$

Solving for  $P$ ,

$$P = \frac{TQ_{in} p_a}{h} \quad (52)$$

Using (50) and (52), a more complete definition of (45) can be created:

$$T^3 = \frac{mh^2}{A_c^2 Q_{in} p_a} \quad (53)$$

Appendix A contains typical values for the parameters of the system. Plugging these values into (50), (52), and (53) shows that the scale of  $P$  is several orders of magnitude higher than the scale of  $Z$  and  $T$ .  $P$  has an order of tens of thousands of Pascals while  $Z$  and  $T$  have a scale of thousandths of meters and seconds. The fact that these scales are extremely different indicates that the system is classified as stiff. The full nondimensional system of equations is given in Appendix B.

### 3.3 Stability of the System

Due to the harmonic “forcing” caused by the waves under the cushion, it would not be surprising to see that a possible solution of the system would be a periodic orbit or trajectory. However, it would also be desirable to know if there are any parameters for which the system becomes unstable or the behavior of the periodic solution changes. The stability chart is very useful for deciding what the optimal operating conditions for the

barge would be. However, finding the stability of this system is quite complicated. The differential equation for pressure is non-autonomous and piecewise-nonlinear. The piecewise-nonlinear terms, which are also periodic, lead to some difficulty in characterizing the stability of the system.

In this section, the stability of the system is approached analytically and numerically. There are two parameters which will can practically be varied and will likely change the behavior of the system: the amplitude of the incoming waves  $a$ , and the fan pressure  $p_f$ . The incoming flowrate  $Q_{in}$  and  $p_f$  are related by the following relationship:

$$Q_{in} = \phi A_f \sqrt{\frac{2}{\rho_a} |p_f|} \text{sign}(p_f) \quad (54)$$

The other advantage of varying these parameters is that for certain combinations the system of equations is greatly simplified. For example, for the case where  $a=p_f=0$ , many terms drop out of (40). To find the equilibrium point, the left hand side of our system of ODEs is set to zero. From (32) the equilibrium pressure is found:

$$p_{c,eq} = \frac{mg}{Ac} \quad (55)$$

The equilibrium pressure will not vary for any combination of  $p_f$  or  $a$ . The equilibrium acceleration  $y_{eq}$  is simply equal to zero. For (14),  $y = y_{eq} = 0$ ,  $a = 0$ , and  $Q_{in} = 0$ . Solving for  $z_{eq}$  yields:

$$z_{eq} = \frac{A_f \sqrt{\frac{2}{\rho_a} p_f}}{2(B_c + L_c) \sqrt{\frac{2}{\rho_a} p_{c,eq}}} + H \quad (56)$$

This equilibrium point (54-56) represents an unstable spiral leading to a stable periodic orbit. Fig. 18 shows that when the initial conditions are moved slightly away from the equilibrium, the system enters a greater orbit. This is due to the pressure terms on the left hand side of (40). This is the simplest case for the system.

When the fan begins to supply air into the cushion, and waves start interacting with the system, it becomes very impractical to find analytical equilibrium for the system. Appendix C contains a expressions for the equilibrium of the system at nonzero  $a$  and  $p_f$ . A problem arises when solving for  $z_{eq}$ , because it is embedded in non-separable equations. Since one would need to numerically solve the analytic expressions, it is more practical to take the original ODEs and solve them numerically to get the “brute-force” solution. Since the system has been classified as stiff by examining the nondimensionalization, the system can be solved using the built-in MATLAB function ODE15s.

As can be seen in Fig. 18, the solution can be visually dense and complicated, and it is possible that some behavior is being missed. To get a clearer look at the system, a map is created based on a surface of section in the  $x$ - $y$  plane (see [4]). The section was chosen to be at the elevation of  $p_f$ . The zero-upcrossing points of the system through the section are plotted to create the map.

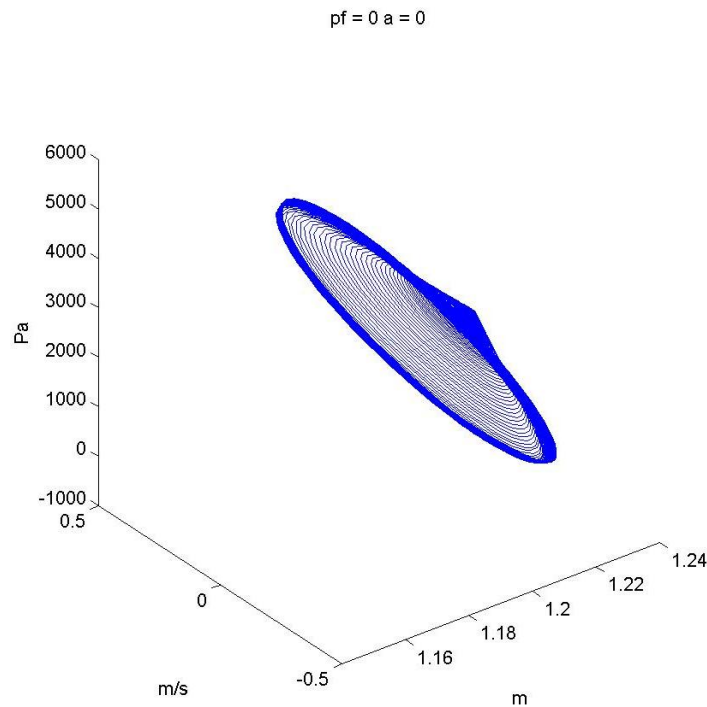


**Figure 18.** Stable spiral.  $P_f$  has units Pa, and  $a$  is meters of wave amplitude.

A Poincaré map was considered due to the harmonic component of the waves. However, the addition of the internal forcing of the cushion pressure means the system never oscillates at an unknown frequency (it is not the frequency of the incoming waves). Fig. 19 shows the intersection of Fig. 18 on the surface of section. There are some transient points, but as the system reaches steady state the intersections approach the periodic orbit.

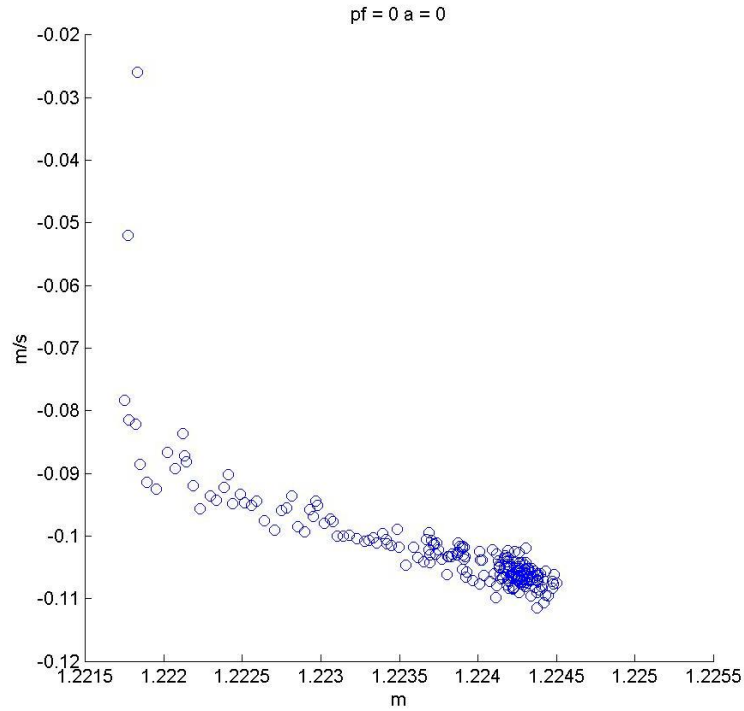


**Figure 19.** Intersections on the surface of section for Fig. 18.

Using the method described above, the system parameters  $a$  and  $p_f$  are varied to explore the stability of the system. Appendix D contains an exhaustive collection of trajectories and surfaces of section. Moving through the parameters reveals the following behavior: the system first transitions from a periodic solution into quasiperiodic solutions; and as  $a$  increases further, there are period bifurcations, with the appearance of super harmonics in the surface of section.

The quasiperiodic solution is found by seeing the intersections on the surface of section move along a closed path. Fig. 20 shows the system with a quasiperiod solution,

with some outlying transients. Increasing the parameters further, the quasiperiodic solution gives way to a period-doubling bifurcation (Fig. 21).

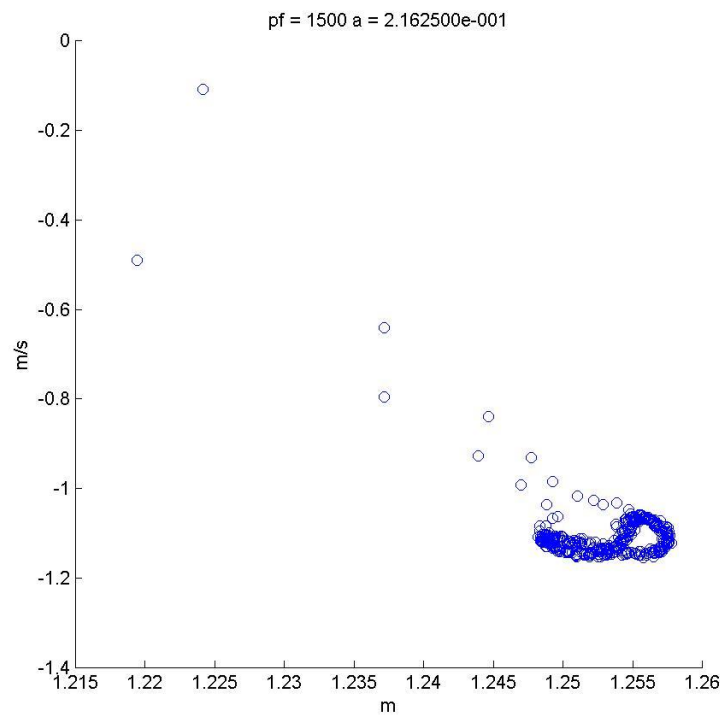


**Figure 20.** A quasiperiodic solution.

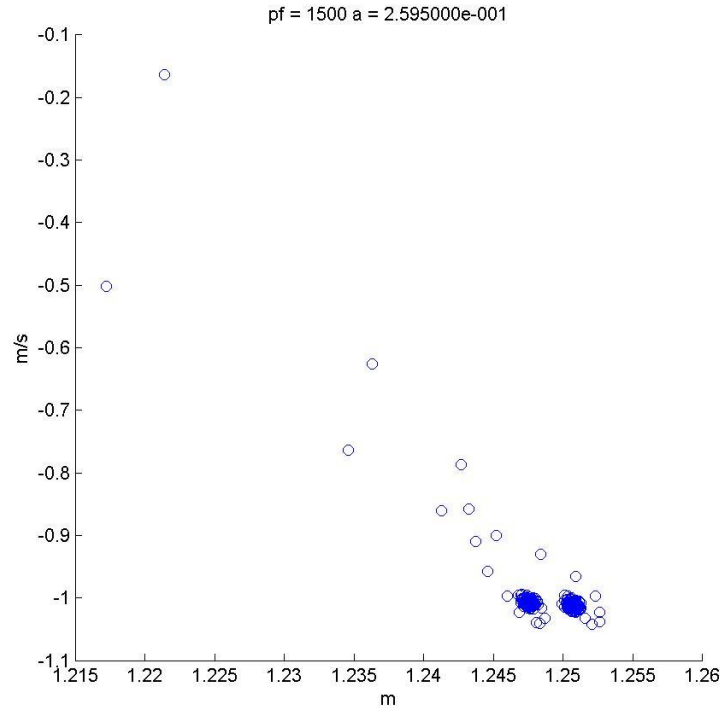


**Figure 21.** Development of multiple-period solution.

Examining Appendix D, it seems that varying  $p_f$  only changes the location of the intersections. The main source of the bifurcations is the varying of the wave amplitude  $a$ . Increasing the wave amplitude further leads to more period doublings and chaotic behavior. It should be noted that as at some wave amplitudes, the chaotic behavior clears to a solution of less harmonics. The overall character of the bifurcations is an intermittent, period-doubling route to chaos. Fig. 22 shows a rough sketch of the bifurcation diagram for the system.

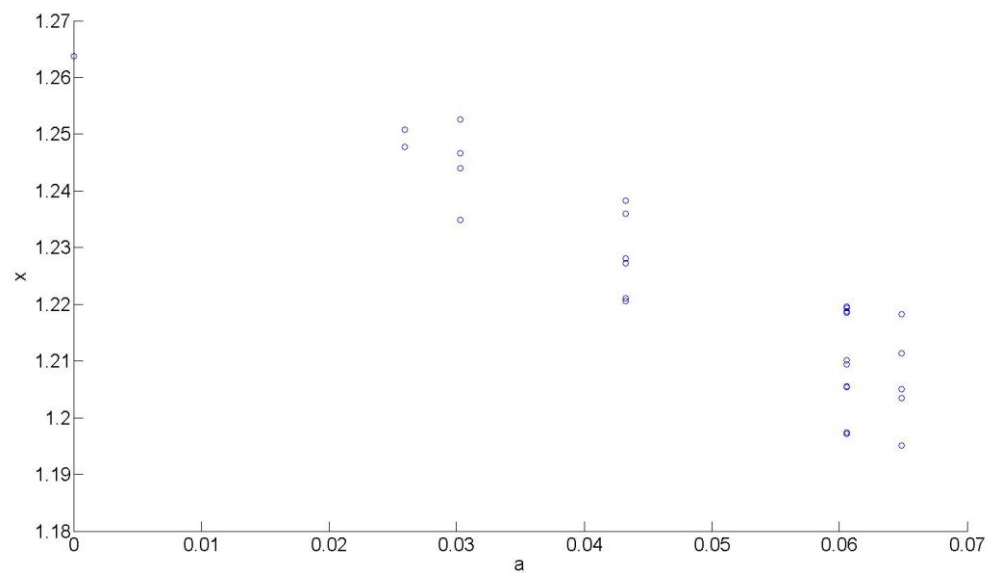


**Figure 22.** Sketch of bifurcation diagram. Note, the spaces in between the plotted values had too many transients to be used. Future simulations should be run longer.



#### 4. CONCLUSION

The method of Lee and Newman (2000) has been applied to the case of the T-Craft using the low-order panel module of WAMIT. The method involves the addition of air cushion boundary conditions based on Fourier modes, designed to approximate the elevation of the water level in the air cushion.

The low-order results are benchmarked against the computational barge results of Pinkster et al. (1998), and the experimental results of Bishop et al. (2010). This potential method is well-established, and the benchmarks support the validity of the simulations, despite simplifications to the air cushion. Reviewing the comparisons between the data of the T-Craft on its cushion and off its cushion, it is unsurprising that there are significant differences in the seakeeping performance. Some degrees of freedom are amplified while on the cushion, such as the roll, sway, and yaw. These motions will affect the interaction between the ship and the seabase ramp structures.

This paper studied the behavior of an air cushion system in the time-domain for a regular wave environment. Starting with a system of equations for either the vertical longitudinal or transverse planes, the system was simplified to equations for the heave motion of the cushion. Despite the simplifications, the system must be solved numerically. The system was reformed into a system of ordinary differential equations. Nondimensionalization was performed to compare the scales of the state space variables, namely the pressure, heave, and heave velocity. Examining the numerical solution over a variation of the wave amplitude and fan pressure, several bifurcations were found, and a plot of these bifurcations was created. The system transitions from a periodic orbit, to

subharmonic orbits, to multiple-period solutions. The period-doubling increases to eventual chaos.

One focus of future work would be making the system more realistic. By including the hydrostatic effects of the hull, the systems of equations can be modified to include the pitch and roll motions. The extra two degrees of freedom can be added to the ODEs and solved numerically with little additional difficulty. The geometry of the hull can be made more realistic. Another improvement is replacing the constant  $Q_{in}$  with a flowrate calculated from characteristic equations of the intake fan. The fluctuating  $Q_{in}$  is a function of the cushion pressure, which makes (14) a recursive equation. Therefore,  $Q_{in}$  must be solved at every time step.

One application of this paper is modeling the seakeeping of the ship. Taking the Fourier transform of the time-domain solutions calculated, the spectrum of the exciting force is obtained. From the spectrum,  $X_i(\omega)$  is found and put into (1). Calculating the hydrodynamic coefficients, the transfer functions between the spectrum of the waves and the spectrum of the cushion motion can be solved. This will allow comparison between the linear potential model and the nonlinear dynamic model. One case in which this is useful is shown in Fig. 23. Here, a ship supported by an aircushion moves towards the beach. Water waves in shallow water are subject to shoaling; as the waves approach the shore the amplitude  $a$  increases before eventually breaking. As was seen in this paper, the stability of the ship is greatly affected by the wave amplitude. By understanding the system, the vibrations in the air cushion can be minimized while approaching the shore.

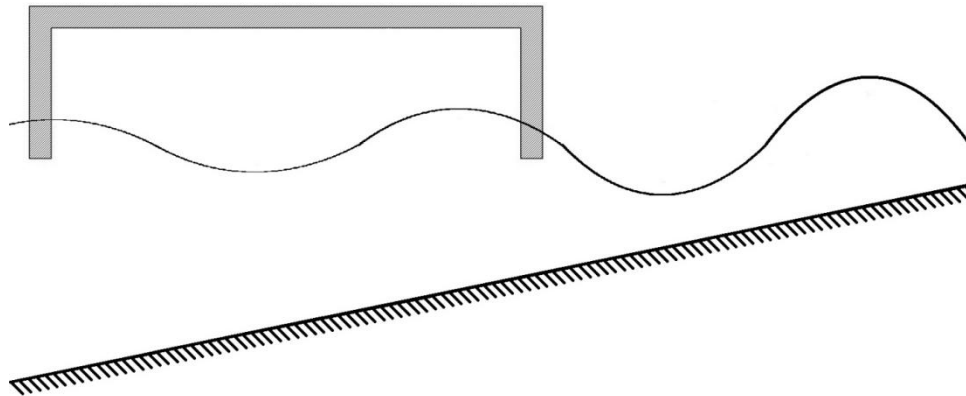


**Figure 23.** An air cushion ship moving in shallow water.

Either of the two models studied can be used for control applications. ACV's are usually controlled by manipulation of the air pressure inside the cushion, which is sometimes known as "ride control" (Faltinsen, 2005). The manipulation of the cushion pressure can control the heave and pitch of the vessel. In the future, these simulations will be coupled with the seabase and have positioning control to reduce relative motions of the individual bodies and reduce connecting loads.

## REFERENCES

- Bishop, R.C., Silver, A.L., Tahmasian, D., Lee, S.S., .Park, J.T, Snyder, L.A., and Kim, J., 2011. TCraft Seakeeping Model Test Data Report-Update. Naval Surface Warfare Center, Caderock Division, Bethesda, Maryland. Hydro-mechanics Department Report 50-TR–2010-062.
- Faltinsen, O.M., and Tore, U., 1998. Cobblestone Effect on SES. Symposium on Fluid Dynamics Problems of Vehicles Operating near or in the Air-Sea Interface. Procedures of Research and Technology Organization, Applied Vehicle Technology Panel, Amsterdam.
- Faltinsen, O.M, 2005. Surface Effect Ships. Hydrodynamics of High-Speed Marine Vehicles. Cambridge University Press, pp. 141-64.
- Hughes, M.J., and Silver, A.L., 2010. Method of Evaluation of Multi-Vessel Surface Effect Ship Motion Prediction Codes. Naval Surface Warfare Center, Caderock Division, Bethesda, Maryland. Hydro-mechanics Department Report.
- Lee, C.H., and Newman, J.N., 2000. Wave Effects on Large Floating Structures with Air Cushions. Marine Structures 12, pp. 315-30.
- Lee, C.H., and Newman, J.N., 2006. WAMIT® User Manual.  
<<http://scholar.google.com/scholar?hl=en&btnG=Search&q=intitle:WAMIT+user+manual#0>>
- Pinkster, J.A., Fauzi, A., Inoue, Y., and Tabeta, S., 1998. The Behaviour of Large Air Cushion Supported Structures in Waves. Proceedings of the Second International

Conference on Hydroelasticity in Marine Technology. Hydroelasticity in Marine Technology, Fukuoka, Japan, pp. 497-505.

Sullivan, P.A., Byrne, J.E., and Hinchey, M.J., 1985. Non-Linear Oscillations of a Simple Flexible Skirt Air Cushion. *Journal of Sound and Vibration* 102 (2), pp. 269-83.

Yun, L., and Bliault, A., 2000. *Theory and Design of Air Cushion Craft*. Arnold, London.

Zhou, W.L., Hua, Y., and Yun, L., 1980. Nonlinear Equations for Coupled Heave and Pitch Motions of Surface Effect Ships in Regular Waves. *Procedures of Canadian Air Cushion Technology Society International Conference*, Ottawa, pp. 328-359.

## APPENDIX A

## NONDIMENSIONAL FORM OF TIME-DOMAIN MODEL

$$m \frac{d^2 x}{d\tau^2} \frac{Z}{T^2} = A_c p_c - mg$$

$$y = \frac{Z}{T} \frac{dx}{d\tau}$$

$$\begin{aligned} \frac{dq}{d\tau} \frac{PV_c}{T\gamma(Pq + p_a)} &= \phi A_f \sqrt{\frac{2}{\rho_a}} p_f \\ &- \phi \sqrt{\frac{2}{\rho_a}} |Pq| \text{sign}(Pq) B_c \left( \frac{Zx - H - \text{asin}\left(\omega_e T\tau - k \frac{L_c}{2}\right) + \left|Zx - H - \text{asin}\left(\omega_e T\tau - k \frac{L_c}{2}\right)\right|}{2} \right. \\ &+ \frac{Zx - H - \text{asin}\left(\omega_e T\tau + k \frac{L_c}{2}\right) + \left|Zx - H - \text{asin}\left(\omega_e T\tau + k \frac{L_c}{2}\right)\right|}{2} \\ &+ \left. \int_{-\frac{L_c}{2}}^{\frac{L_c}{2}} (Zx - H - \text{asin}(\omega_e T\tau - kX) + |Zx - H - \text{asin}(\omega_e T\tau - kX)|) dX \right) - \frac{Z}{T} \frac{dx}{d\tau} \\ &+ \frac{2B_c a \omega_e}{k} \sin\left(\frac{kL_c}{2}\right) \cos(\omega_e T\tau) \end{aligned}$$

## APPENDIX B

## ANALYTICAL EQUILIBRIUM OF TIME-DOMAIN MODEL

**Conditions for (14)***Case I (front and side leaks)*

$$z - H - a \sin\left(\omega t - \frac{kL_c}{2}\right) > 0$$

$$z - H - a \sin\left(\omega t + \frac{kL_c}{2}\right) < 0$$

*Case II (rear and side leaks)*

$$z - H - a \sin\left(\omega t - \frac{kL_c}{2}\right) < 0$$

$$z - H - a \sin\left(\omega t + \frac{kL_c}{2}\right) > 0$$

*Case III (front, rear, and portion of side leaks)*

$$z - H - a \sin\left(\omega t - \frac{kL_c}{2}\right) > 0$$

$$z - H - a \sin\left(\omega t + \frac{kL_c}{2}\right) > 0$$

*Case IV (leaking everywhere)*

$$z - H - a \sin\left(\omega t - \frac{kL_c}{2}\right) > 0$$

$$z - H - a \sin\left(\omega t + \frac{kL_c}{2}\right) > 0$$

$$z - H - a > 0$$

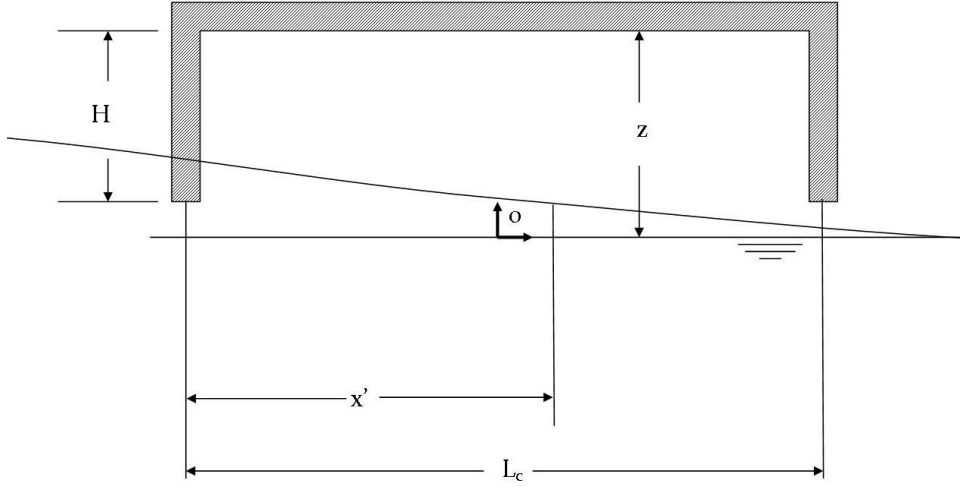
*Case V (not leaking)*

$$z - H - a \sin\left(\omega t - \frac{kL_c}{2}\right) < 0$$

$$z - H - a \sin\left(\omega t + \frac{kL_c}{2}\right) < 0$$

$$z - H - a < 0$$

**Equilibrium of (14)***Case I (front and side leaks)*



Applying the conditions for case I into (14)

$$0 = Q_{in} - \alpha \left[ B_c \left( z - H - a \sin \left( \omega t - \frac{kL_c}{2} \right) \right) + \int_{-L_c/2}^{L_c/2} (z - H - a \sin(\omega t - kx) + |z - H - a \sin(\omega t - kx)|) dx \right] - \beta \cos(\omega t)$$

From the figure, there is only a portion of the air cushion exposed to leaking. Altering the limits of the integral,

$$0 = Q_{in} - \alpha \left[ B_c \left( z - H - a \sin \left( \omega t - \frac{kL_c}{2} \right) \right) + \int_{x' - L_c/2}^{L_c/2} (z - H - a \sin(\omega t - kx) + |z - H - a \sin(\omega t - kx)|) dx \right] - \beta \cos(\omega t)$$

Carrying out the integral yields

$$0 = Q_{in} - \alpha \left[ B_c \left( z - H - a \sin \left( \omega t - \frac{kL_c}{2} \right) \right) + 2 \left\{ (z - H)(L_c - x') - \frac{a}{k} \cos \left( \omega t - k \frac{L_c}{2} \right) + \frac{a}{k} \cos \left( \omega t - kx' + k \frac{L_c}{2} \right) \right\} \right] - \beta \cos(\omega t)$$

To find an expression for  $x'$ , the above figure is used



$$z - H - a \sin \left( \omega t - k \left( x' - \frac{L_c}{2} \right) \right) = 0$$

$$x' = -\frac{1}{k} \left( \sin^{-1} \left( \frac{z - H}{a} \right) - \omega t \right) + \frac{L_c}{2}$$

$$z - H < a$$

Substituting the expression for  $x'$

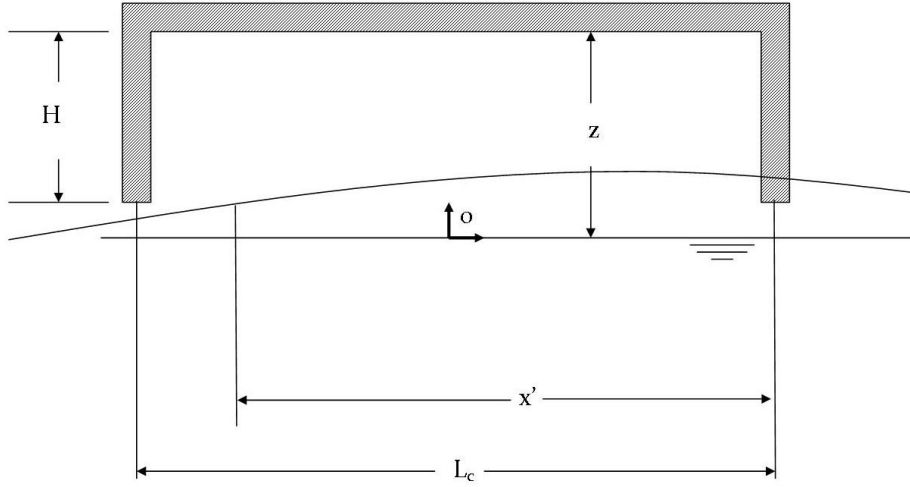
$$0 = Q_{in} - \alpha \left[ B_c \left( \zeta - a \sin \left( \omega t - \frac{k L_c}{2} \right) \right) \right. \\ \left. + 2 \left\{ \zeta \left( \frac{L_c}{2} + \frac{1}{k} \left( \sin^{-1} \left( \frac{\zeta}{a} \right) - \omega t \right) \right) - \frac{a}{k} \cos \left( \omega t - k \frac{L_c}{2} \right) \right. \right. \right. \\ \left. \left. + \frac{a}{k} \cos \left( \sin^{-1} \left( \frac{\zeta}{a} \right) \right) \right\} \right] - \beta \cos(\omega t)$$

where

$$\zeta = z - H$$

Solving for  $\zeta$  will give the equilibrium position of the ship for a given instant of time.

*Case II (rear and side leaks)*



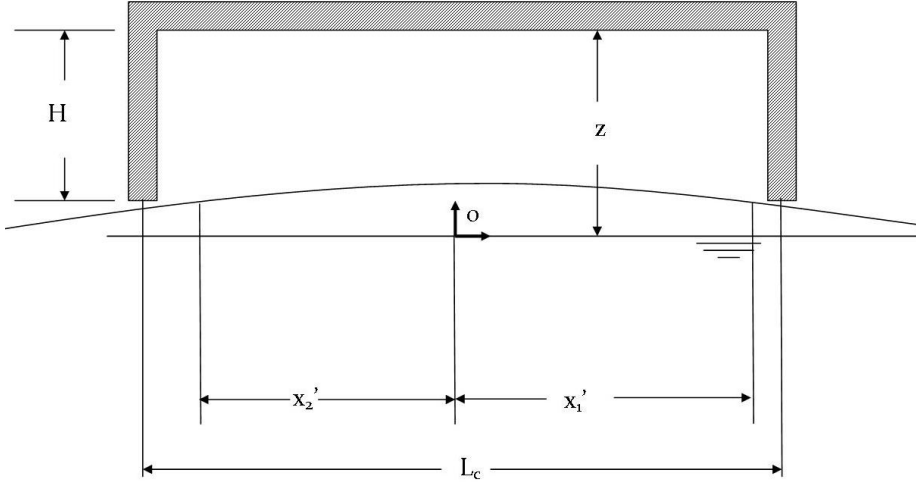
Applying the conditions to (14)

$$0 = Q_{in} - \alpha \left[ B_c \left( z - H - a \sin \left( \omega t - \frac{k L_c}{2} \right) \right) \right. \\ \left. + \int_{-L_c/2}^{L_c/2} (z - H - a \sin(\omega t - kx) + |z - H - a \sin(\omega t - kx)|) dx \right] \\ - \beta \cos(\omega t)$$

Following the procedure for case I

$$\begin{aligned}
0 = Q_{in} - \alpha & \left[ B_c \left( \zeta - a \sin \left( \omega t + \frac{kL_c}{2} \right) \right) \right. \\
& + 2 \left\{ \zeta \left( \frac{L_c}{2} - \frac{1}{k} \left( \sin^{-1} \left( \frac{\zeta}{a} \right) - \omega t \right) \right) - \frac{a}{k} \cos \left( \omega t + k \frac{L_c}{2} \right) \right. \\
& \left. \left. - \frac{a}{k} \cos \left( \sin^{-1} \left( \frac{\zeta}{a} \right) \right) \right\} \right] - \beta \cos(\omega t)
\end{aligned}$$

Case III (front, rear, and portion of side leaks)



Applying the conditions to (14)

$$\begin{aligned}
0 = Q_{in} - \alpha & \left[ B_c \left( 2z - 2H - a \sin \left( \omega t + \frac{kL_c}{2} \right) - a \sin \left( \omega t - \frac{kL_c}{2} \right) \right) \right. \\
& + 2 \int_{-\frac{L_c}{2}}^{-x_2'} (z - H - a \sin(\omega t - kx)) dx \\
& \left. + 2 \int_{-\frac{L_c}{2}}^{-x_2'} (z - H - a \sin(\omega t - kx)) dx \right] - \beta \cos(\omega t)
\end{aligned}$$

Expressions for  $x_1'$  and  $x_2'$  are derived similarly to cases I and II:

$$\begin{aligned}
x_1' &= -\frac{1}{k} \left( \sin^{-1} \left( \frac{z - H}{a} \right) - \omega t \right) \\
x_2' &= \frac{1}{k} \left( \sin^{-1} \left( \frac{z - H}{a} \right) - \omega t \right)
\end{aligned}$$

Carrying out the integrals and substituting  $x_1'$  and  $x_2'$  gives

$$0 = Q_{in} - \alpha \left[ B_c (2\zeta - 2a \sin(\omega t) \cos\left(\frac{kL_c}{2}\right) + 2 \left\{ \zeta \left( L_c - \frac{2}{k} \left( \sin^{-1}\left(\frac{\zeta}{a}\right) - \omega t \right) \right) + \frac{2a}{k} \sin(\omega t) \sin\left(\frac{kL_c}{2}\right) \right\} \right] - \beta \cos(\omega t)$$

*Case IV (everywhere leaks)*

Applying the conditions to (14)

$$0 = Q_{in} - \alpha \left[ B_c \left( 2z - 2H - a \sin\left(\omega t + \frac{kL_c}{2}\right) - a \sin\left(\omega t - \frac{kL_c}{2}\right) + 2 \int_{-L_c/2}^{L_c/2} (z - H - a \sin(\omega t - kx)) dx \right) \right] - \beta \cos(\omega t)$$

Carrying out the integration yields

$$0 = Q_{in} - \alpha \left[ B_c \left( 2z - 2H - a \sin\left(\omega t + \frac{kL_c}{2}\right) - a \sin\left(\omega t - \frac{kL_c}{2}\right) + 2 \left( zL_c - HL_c - \frac{a}{k} \cos\left(\omega t - \frac{kL_c}{2}\right) + \frac{a}{k} \cos\left(\omega t + \frac{kL_c}{2}\right) \right) \right] - \beta \cos(\omega t)$$

Using trigonometric identities and substituting  $\zeta$  for  $z-H$

$$0 = Q_{in} - \alpha \left[ B_c \left( 2\zeta - 2a \sin(\omega t) \cos\left(\frac{kL_c}{2}\right) \right) + 2 \left( \zeta L_c - 2 \frac{a}{k} \sin(\omega t) \sin\left(\frac{kL_c}{2}\right) \right) \right] - \beta \cos(\omega t)$$

Solving for  $\zeta$

$$\zeta = \frac{1}{2\alpha(B_c + L_c)} \left( Q_{in} + 2a\alpha B_c \sin(\omega t) \cos\left(\frac{kL_c}{2}\right) + \frac{4a\alpha}{k} \sin(\omega t) \sin\left(\frac{kL_c}{2}\right) - \beta \cos(\omega t) \right)$$

*Case V (no leaking)*

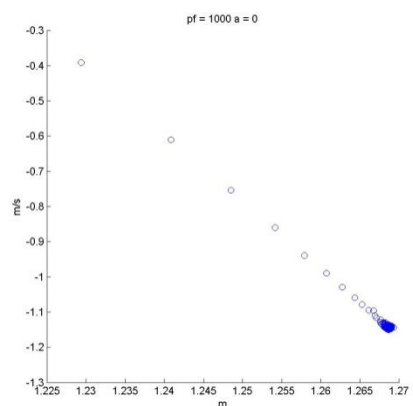
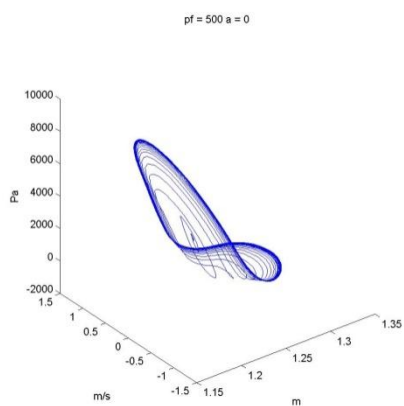
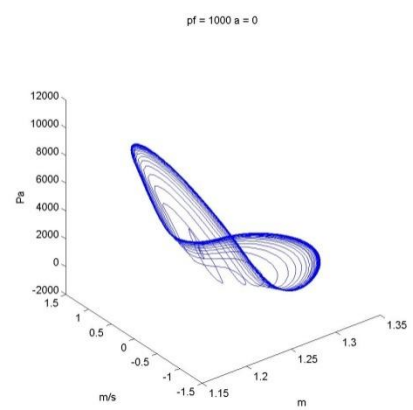
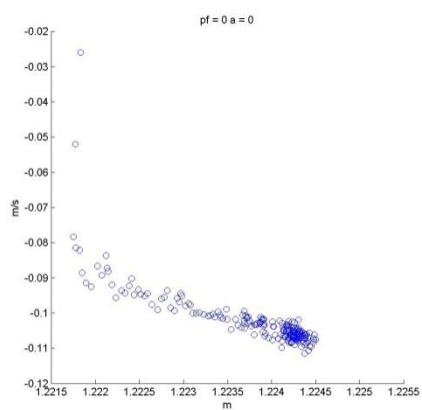
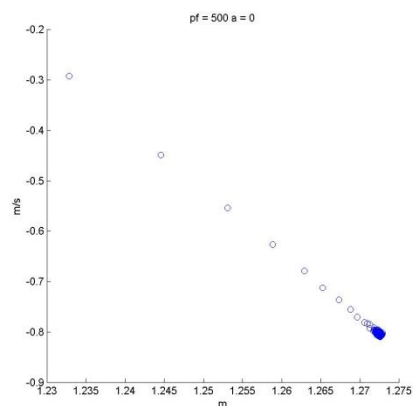
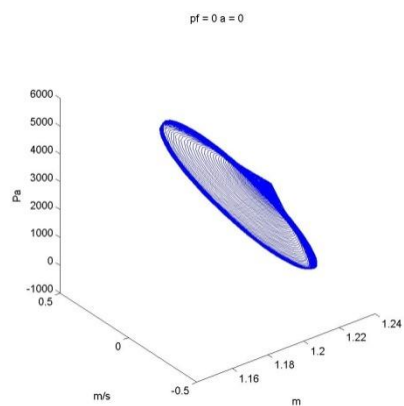
Substituting the condition into (14)

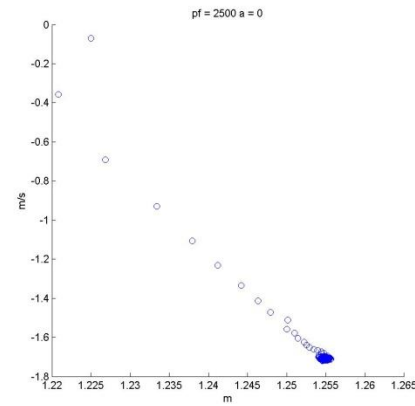
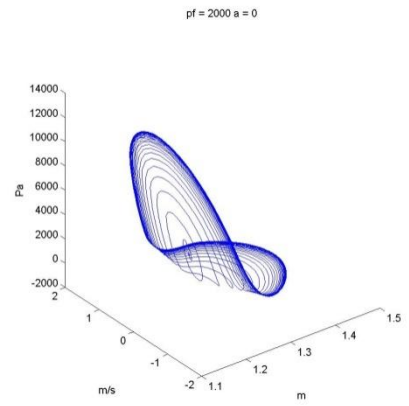
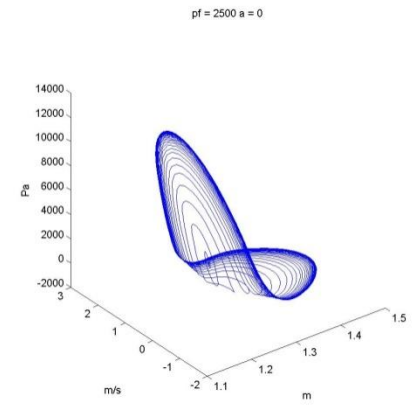
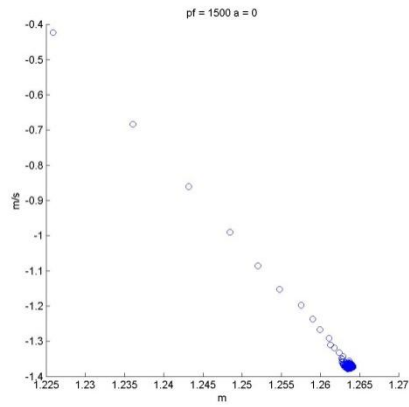
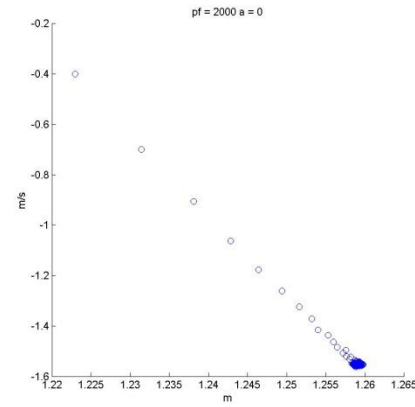
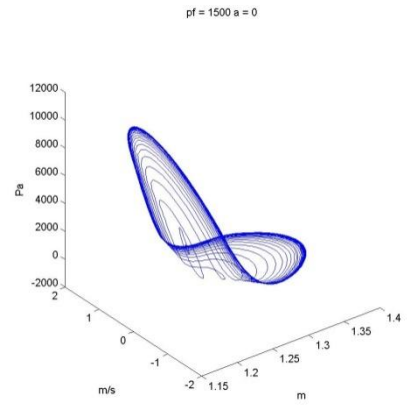
$$0 = Q_{in} - \beta \cos(\omega t)$$

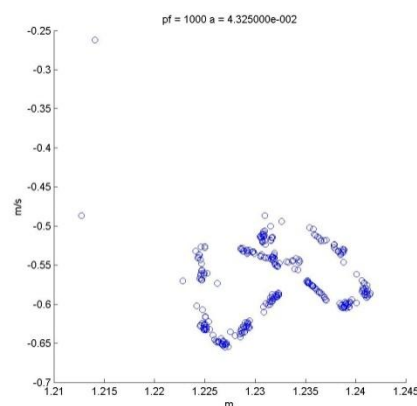
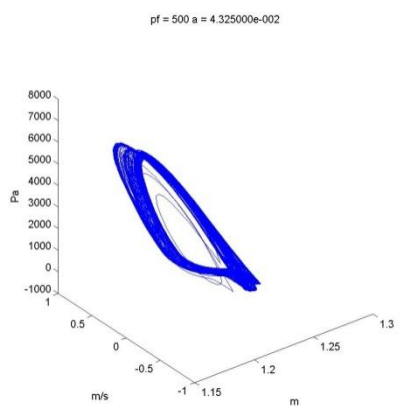
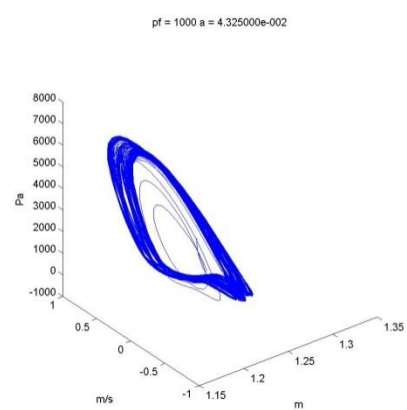
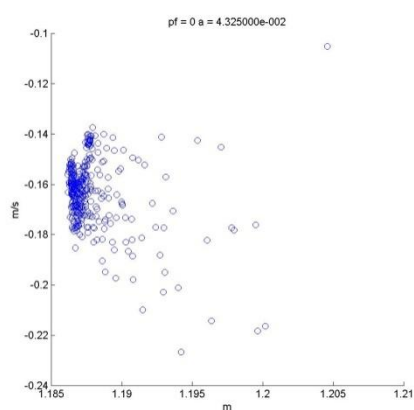
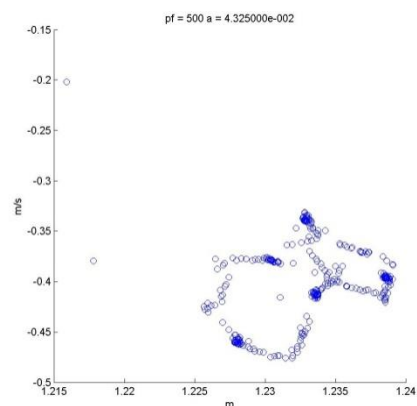
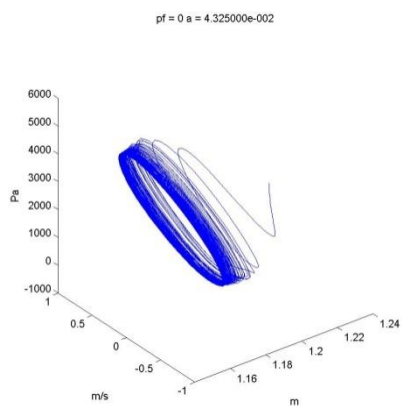
There is no solution for  $\zeta$  or  $z$  here, so there is no equilibrium in this case.

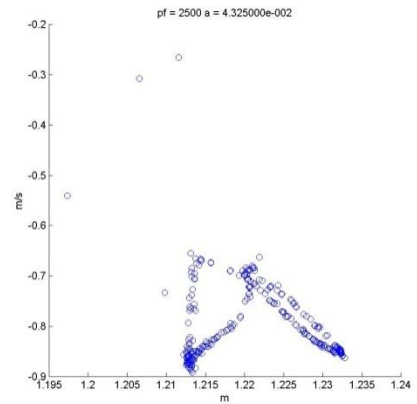
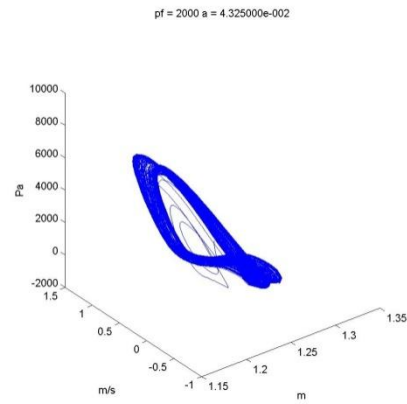
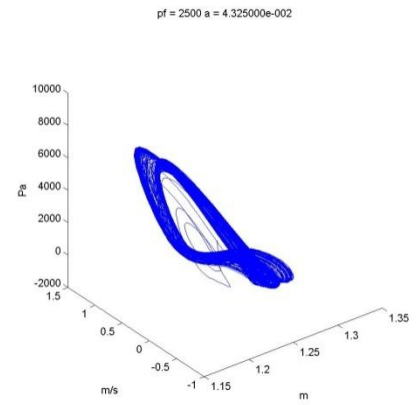
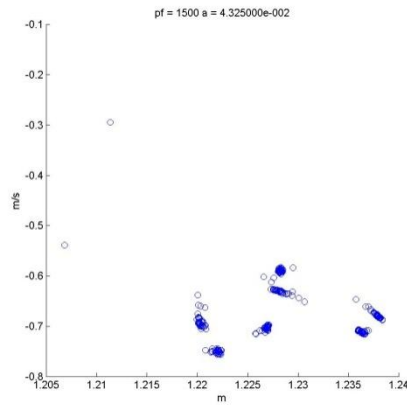
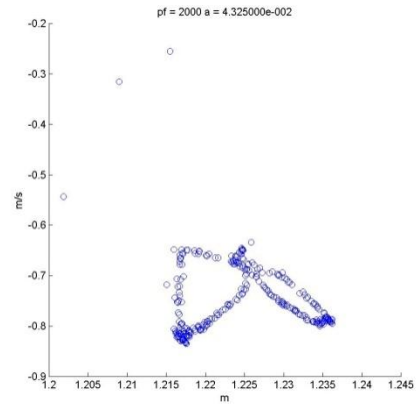
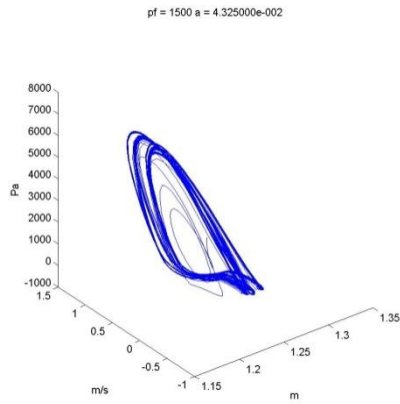
## APPENDIX C

### TRAJECTORIES AND SURFACE INTERSECTIONS OF THE TIME DOMAIN SYSTEM

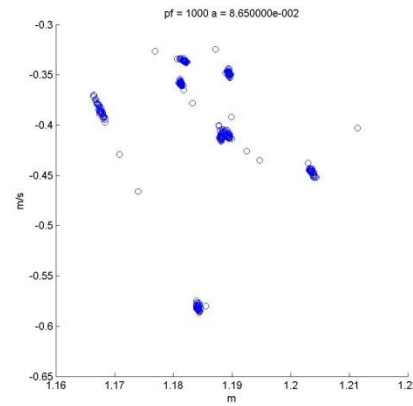
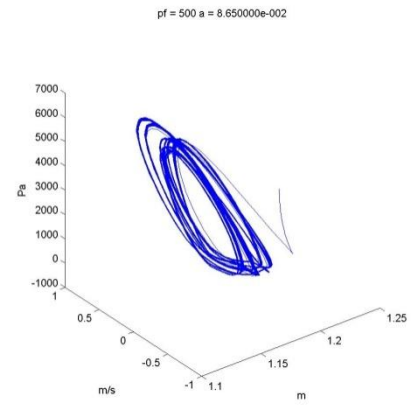
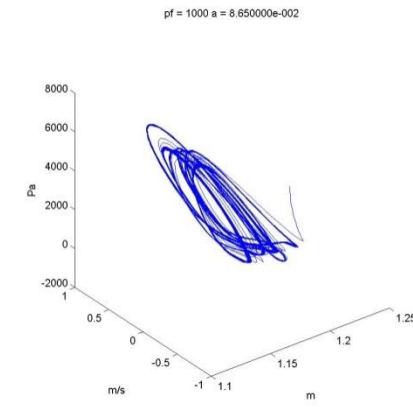
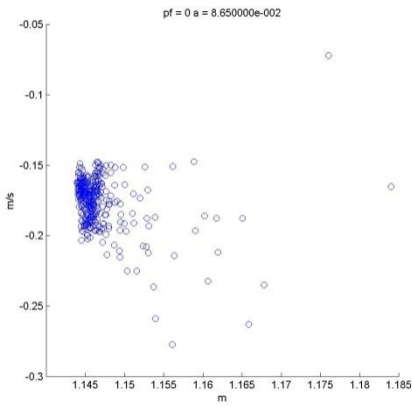
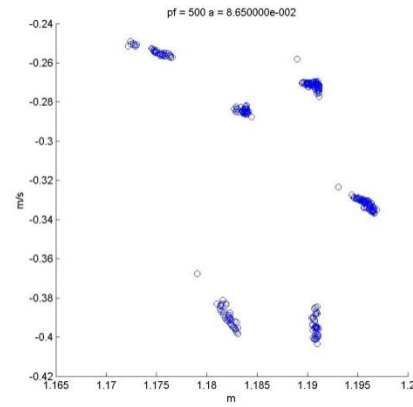
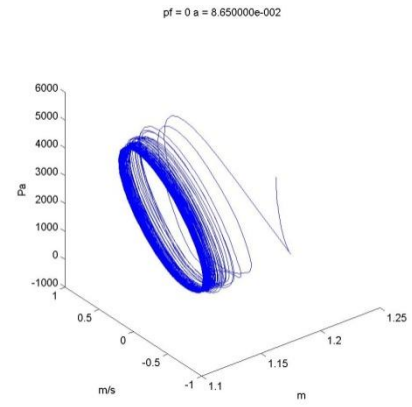


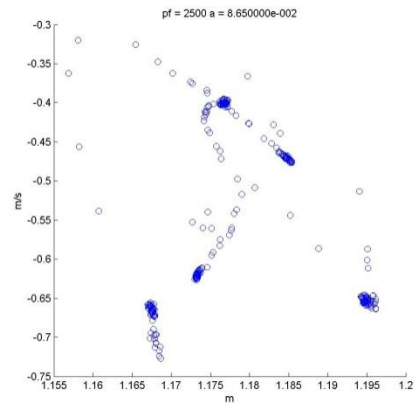
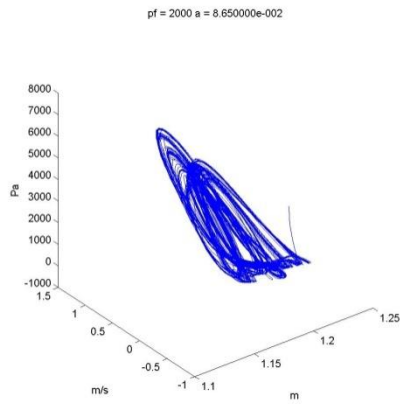
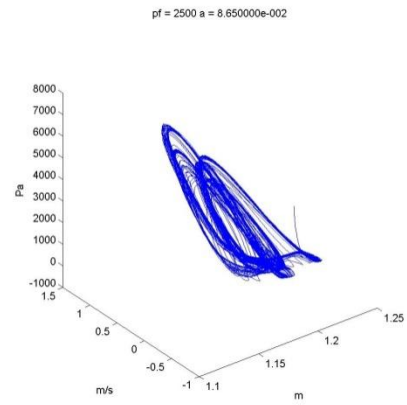
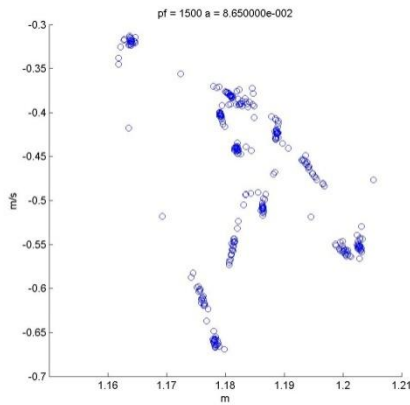
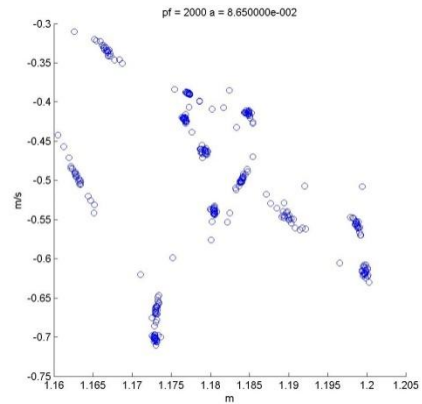
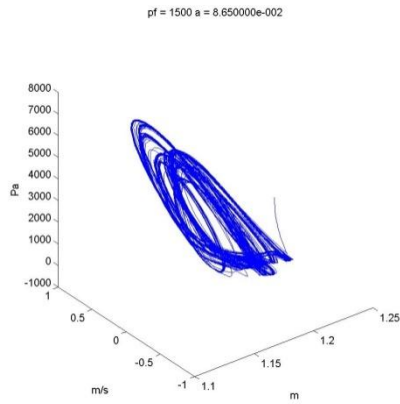


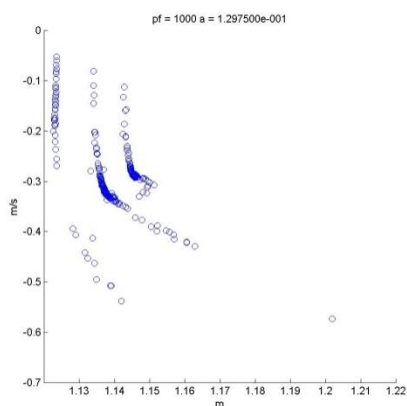
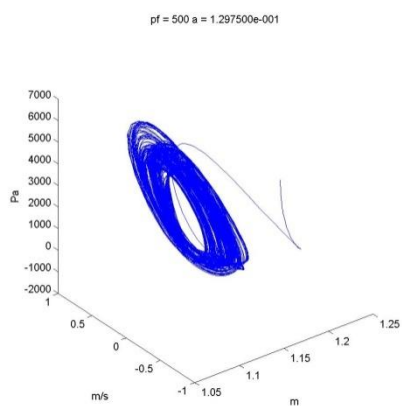
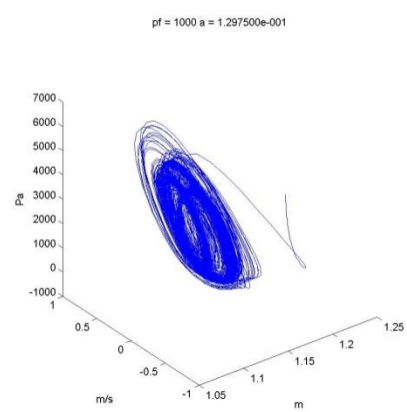
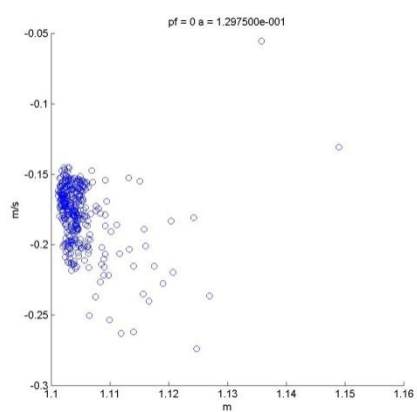
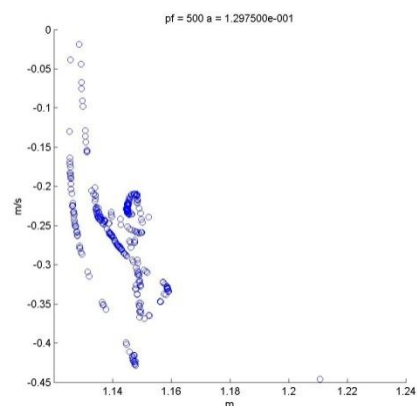
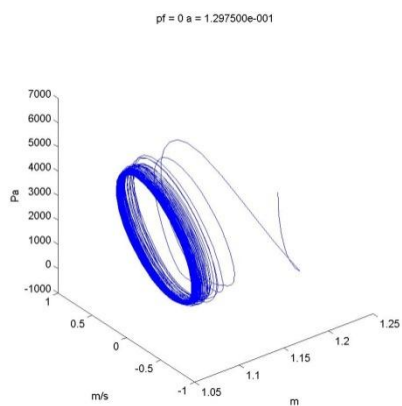


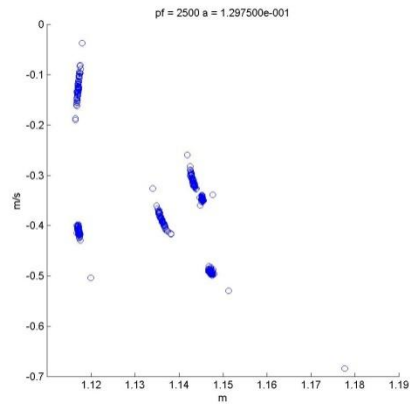
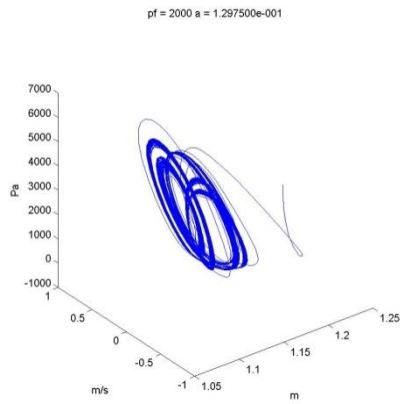
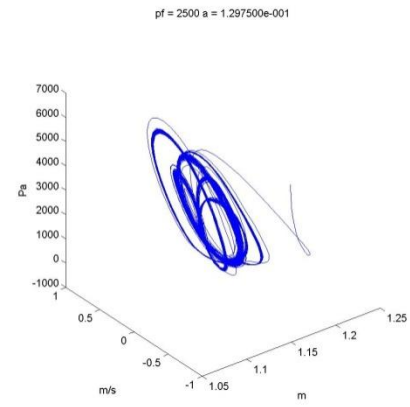
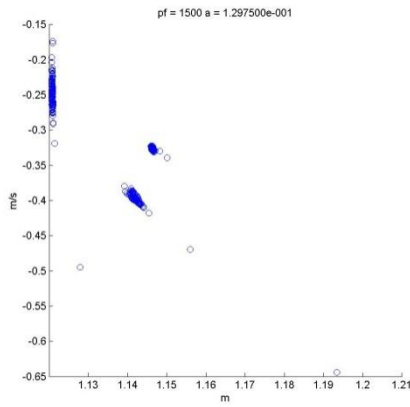
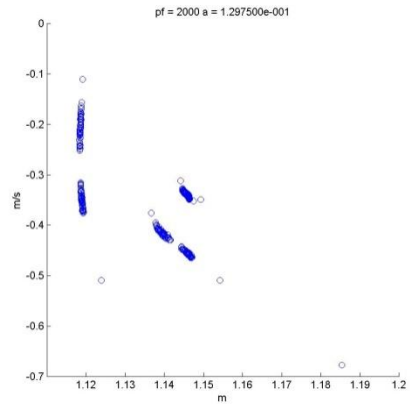
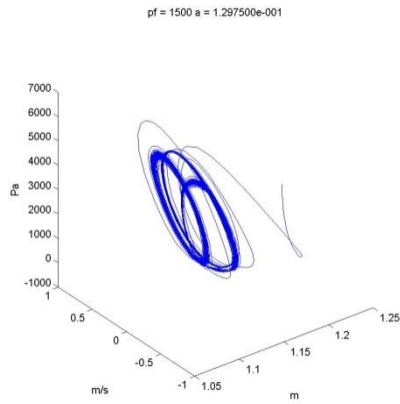


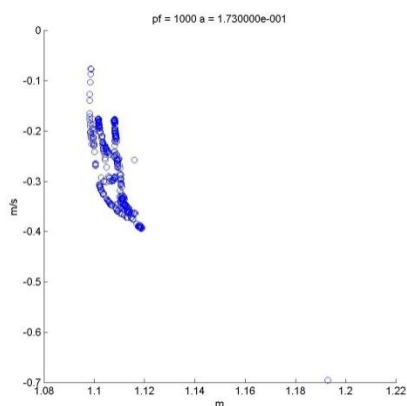
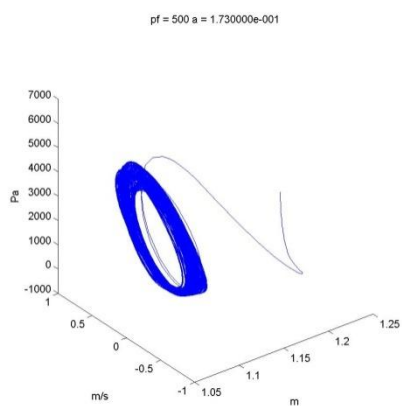
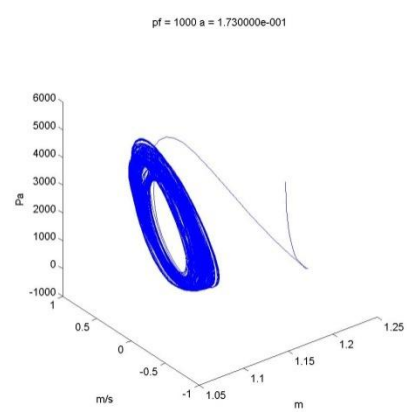
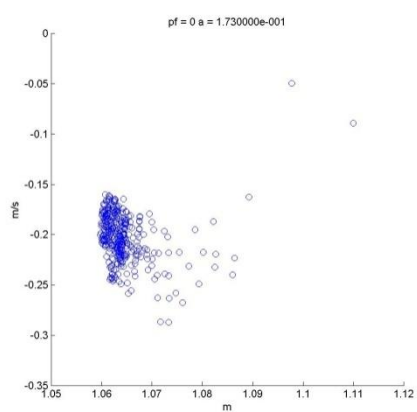
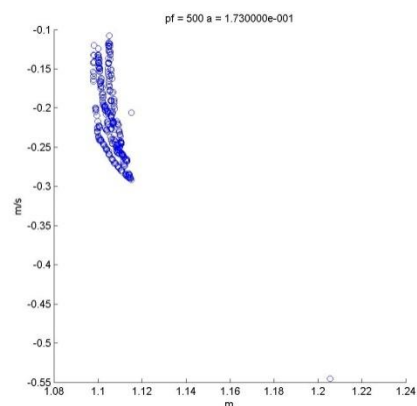
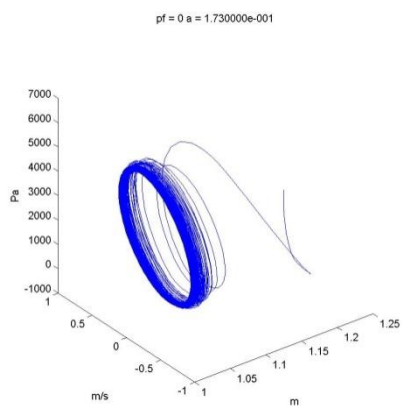


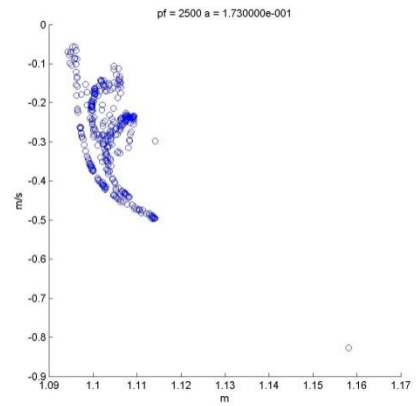
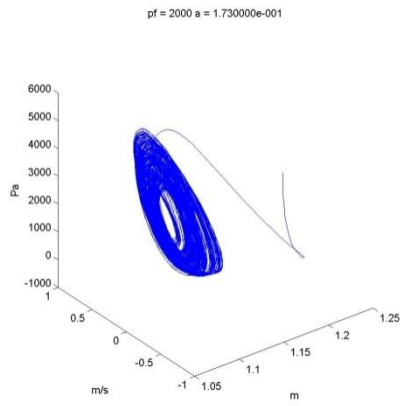
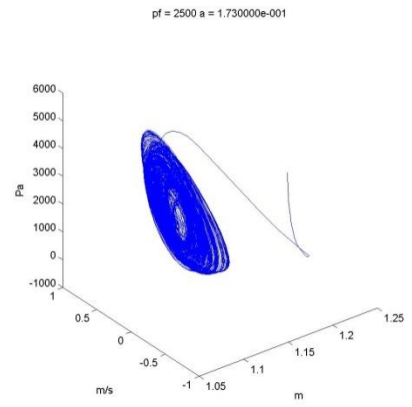
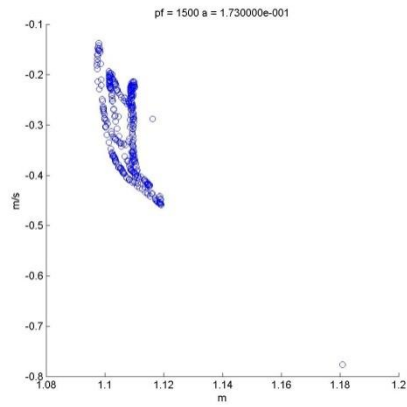
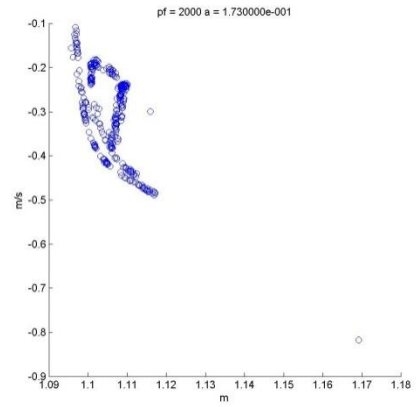
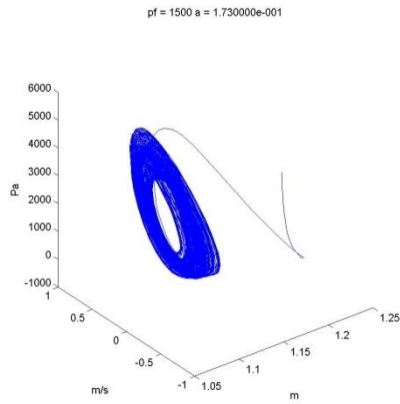


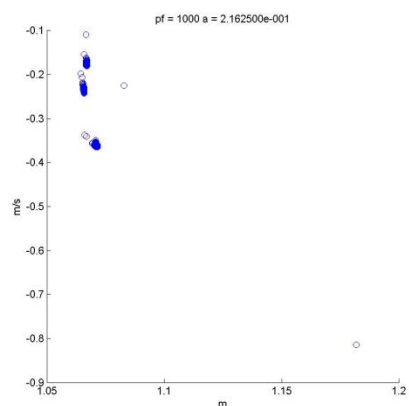
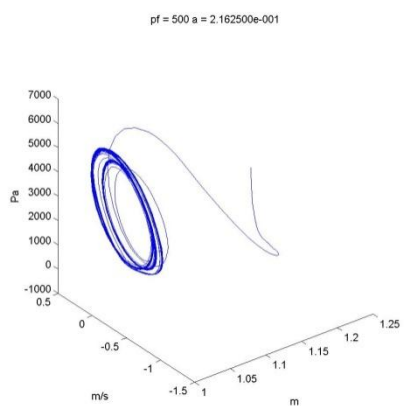
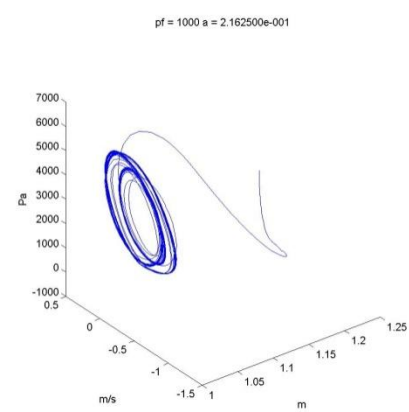
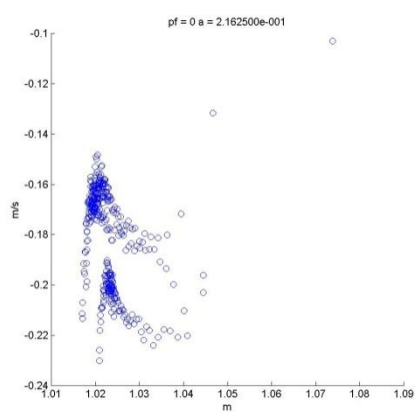
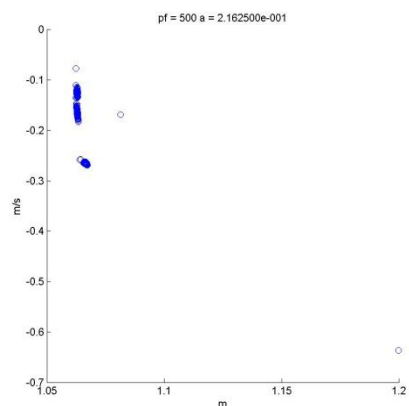
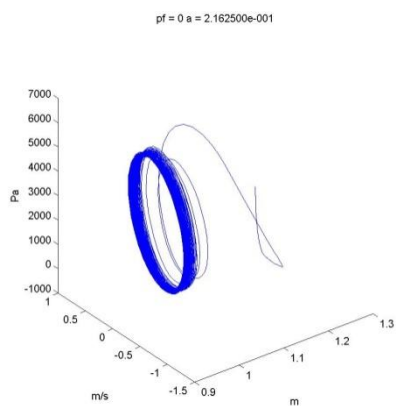


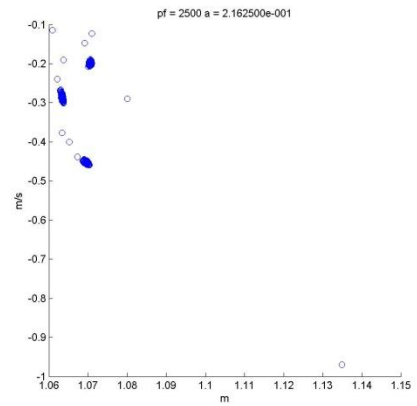
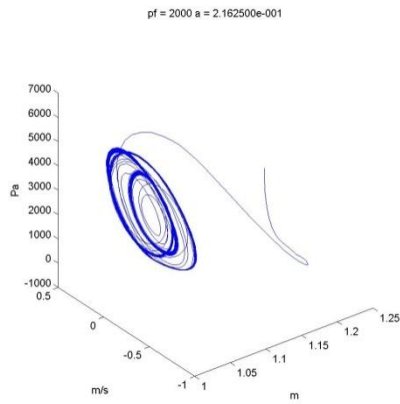
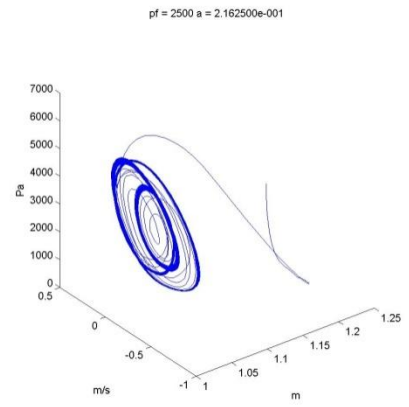
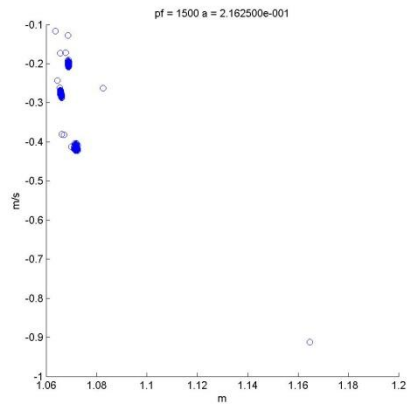
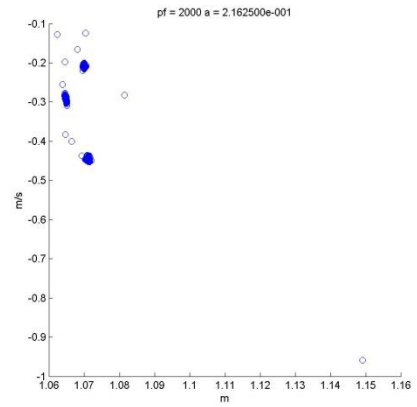
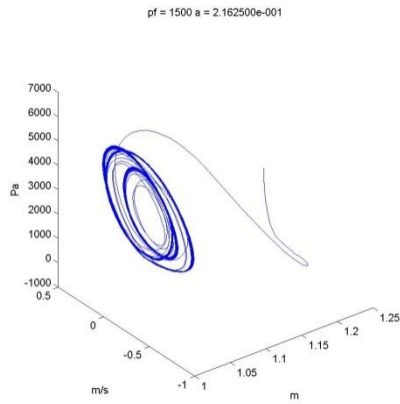




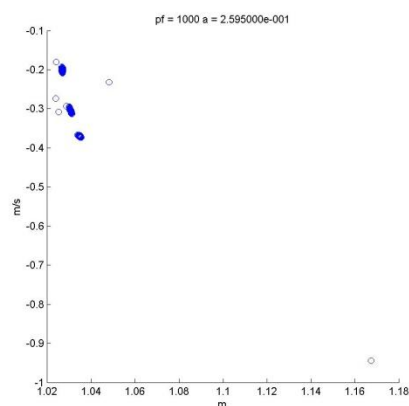
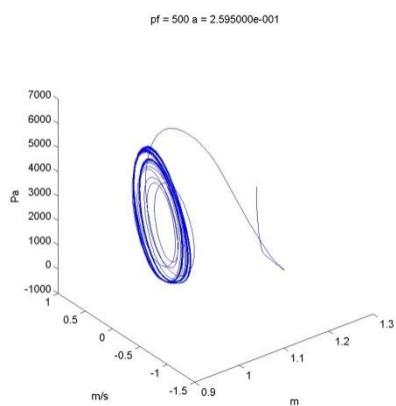
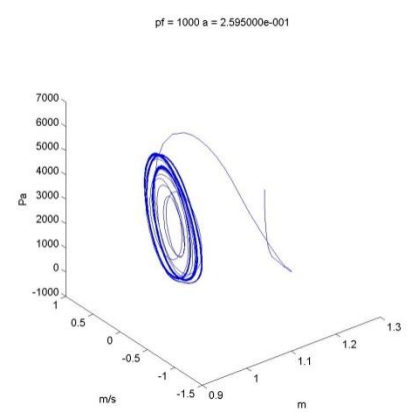
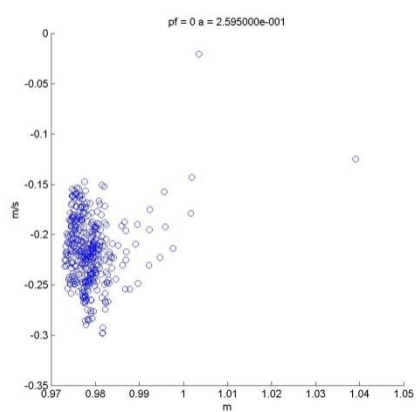
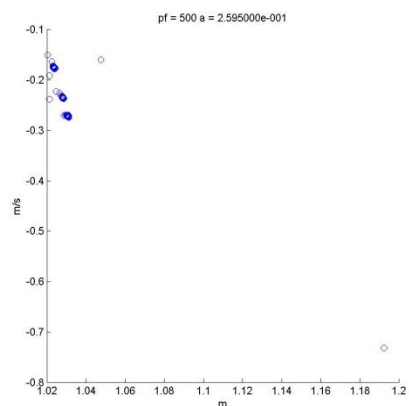
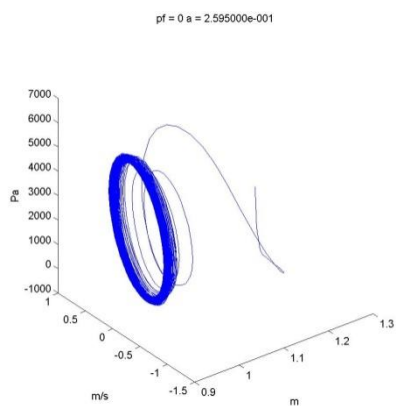


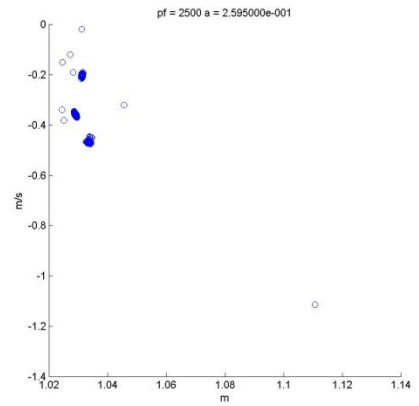
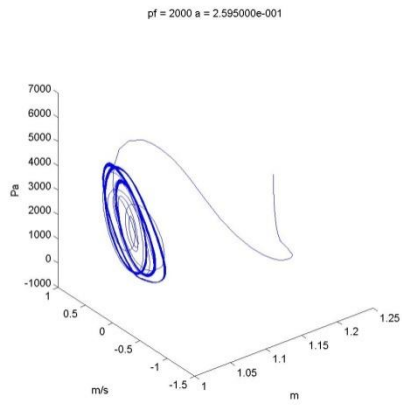
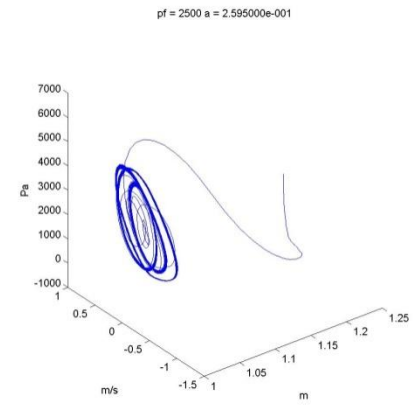
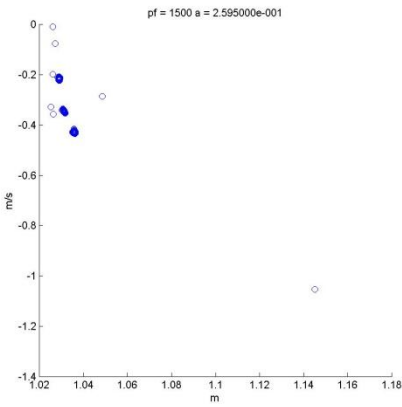
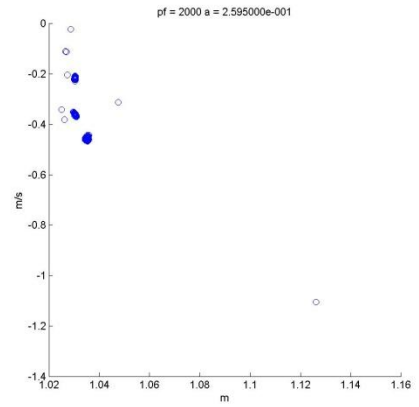
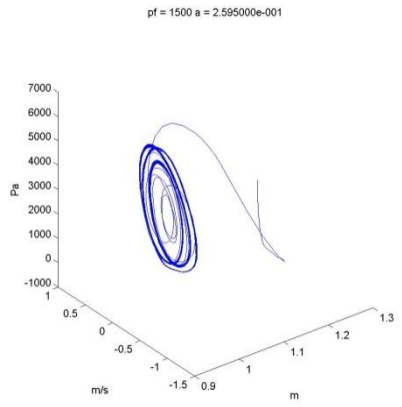


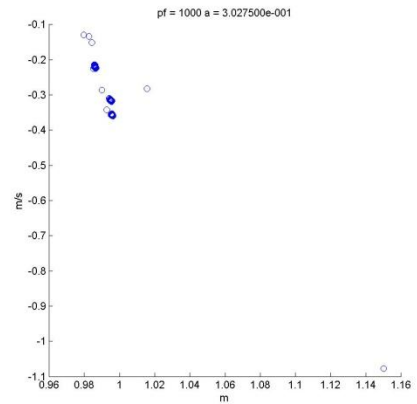
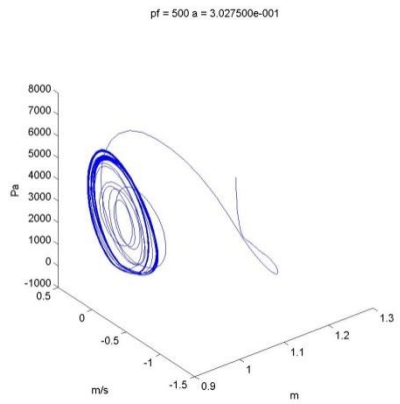
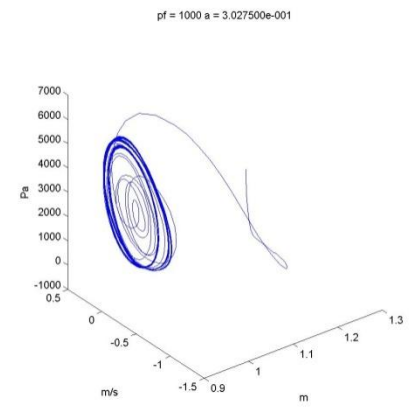
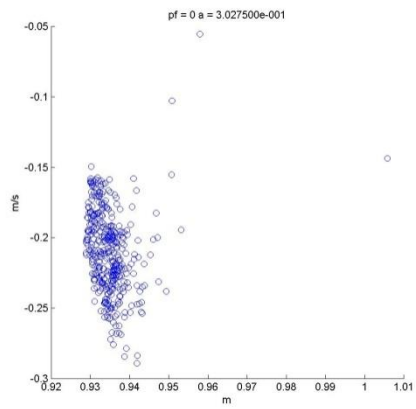
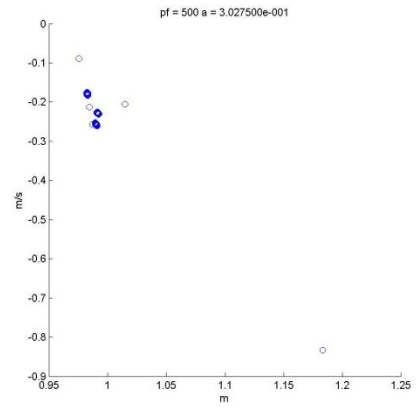
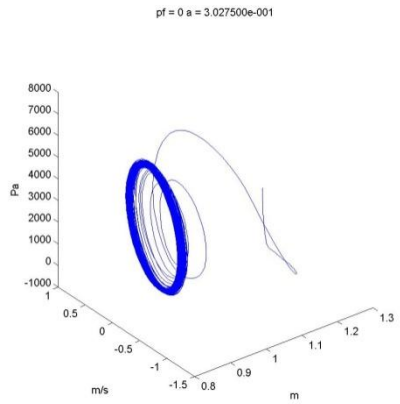


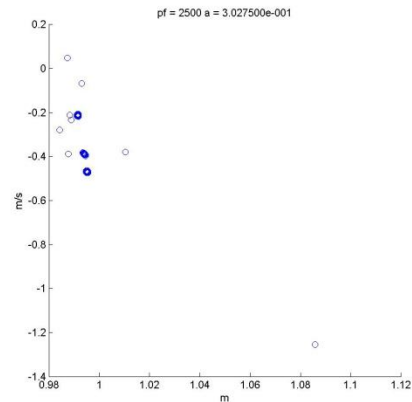
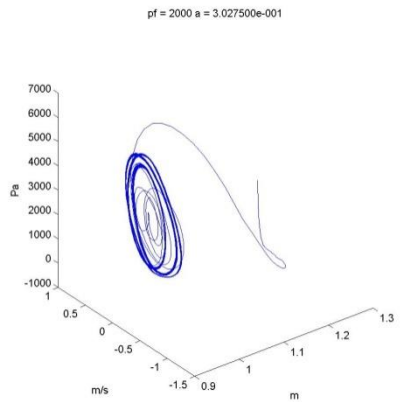
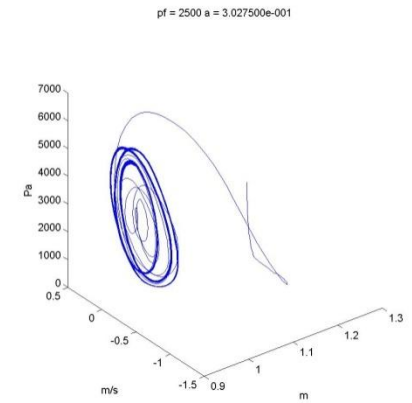
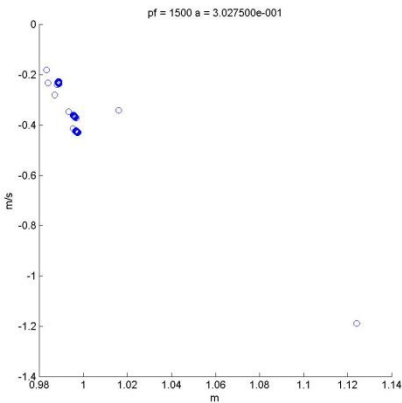
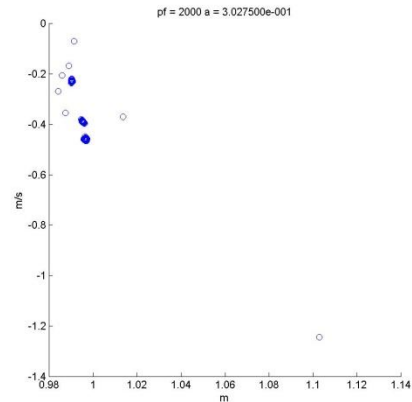
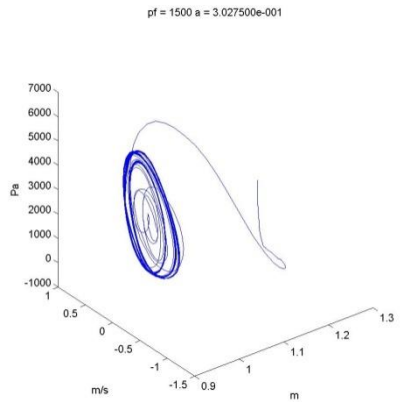


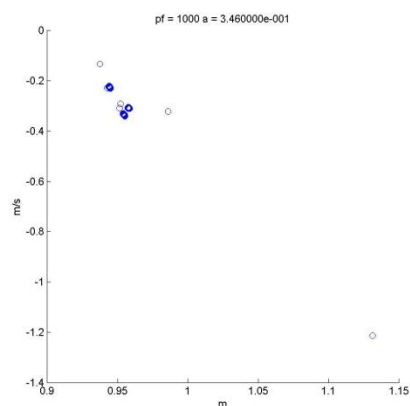
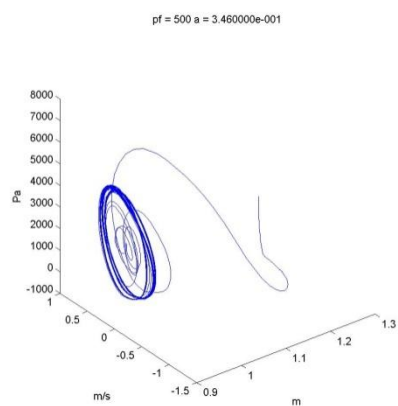
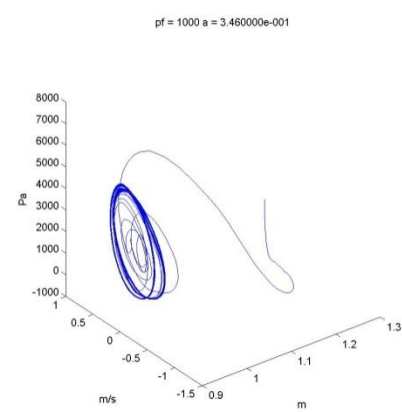
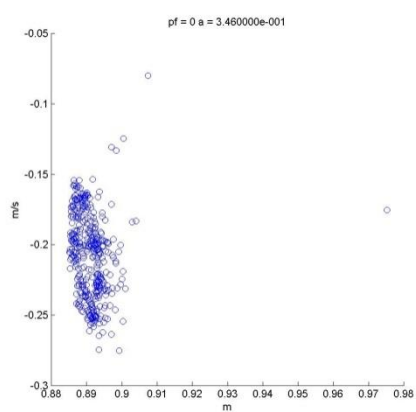
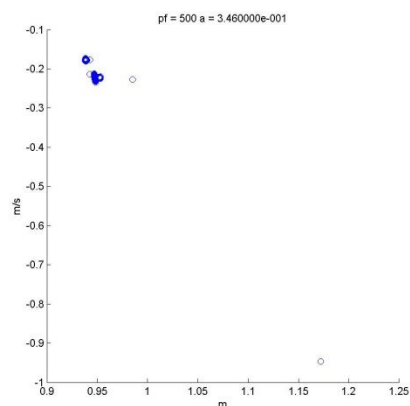
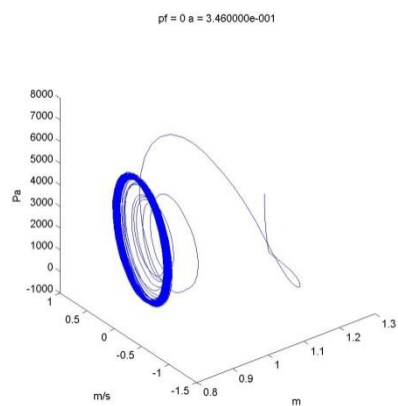


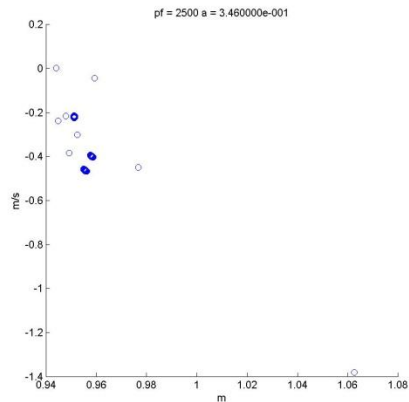
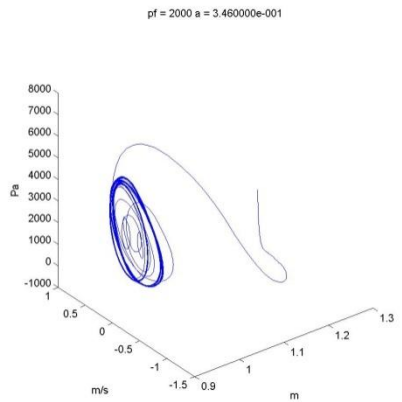
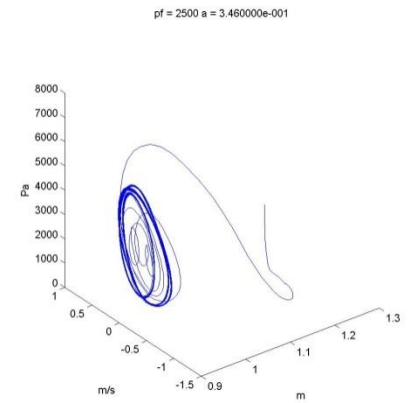
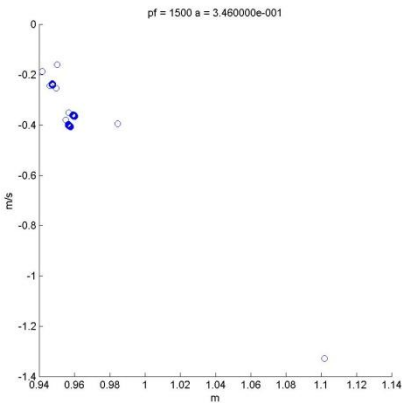
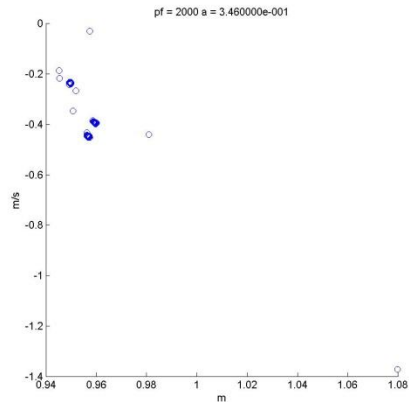
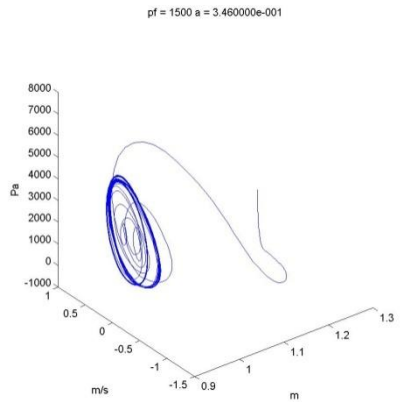


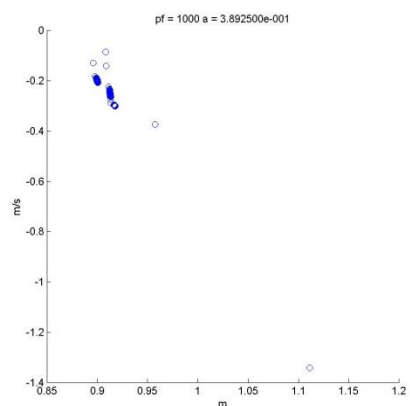
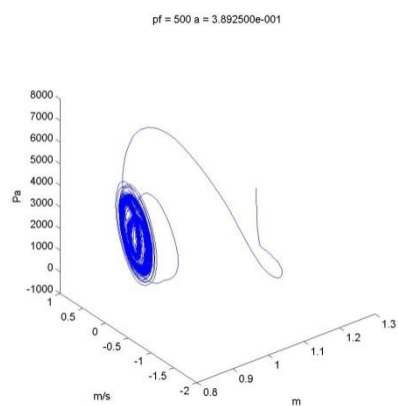
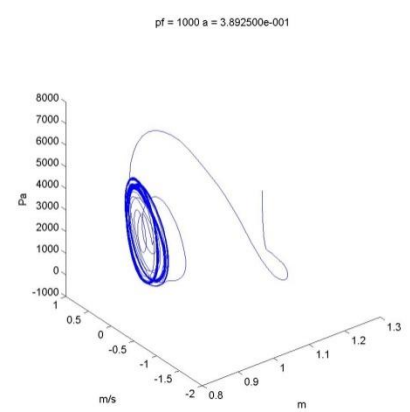
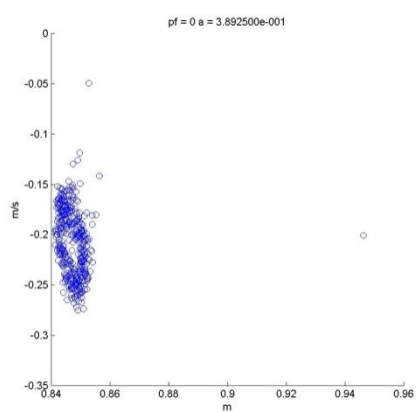
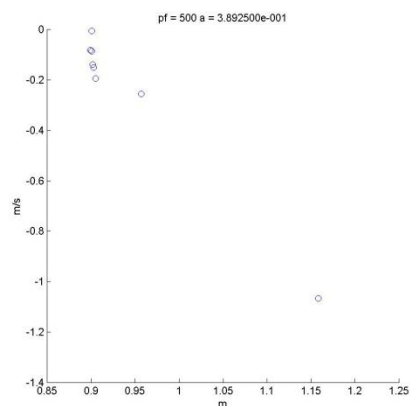
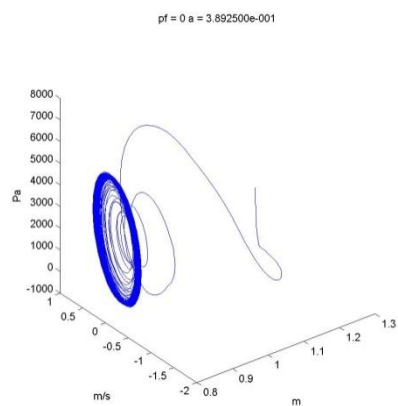


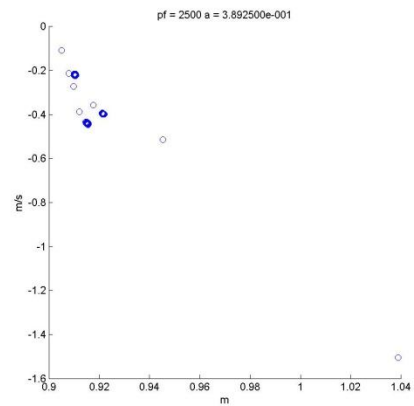
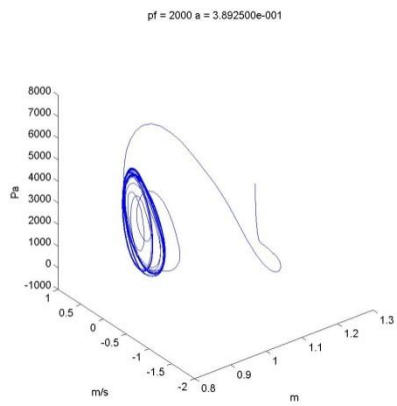
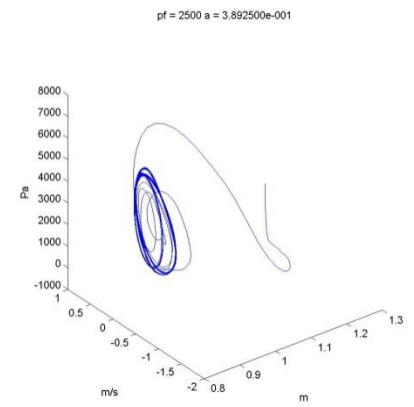
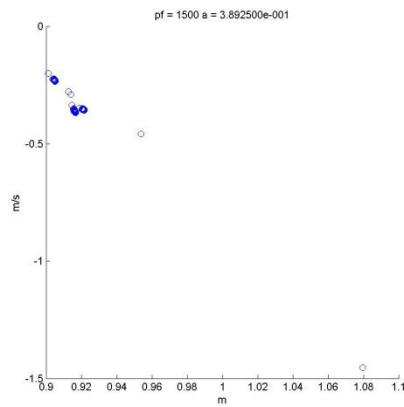
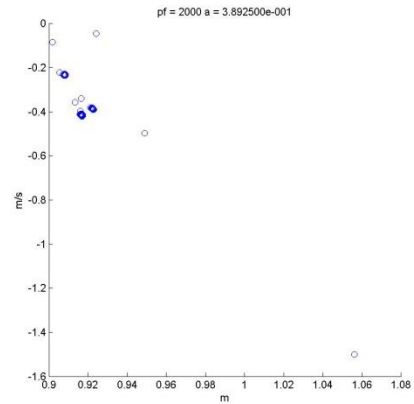
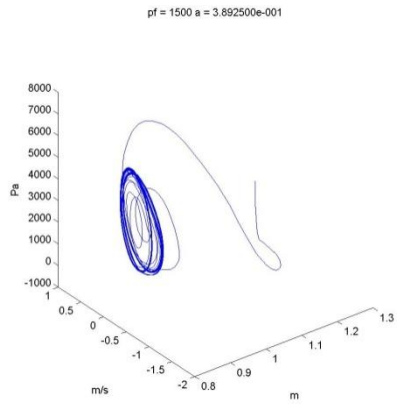




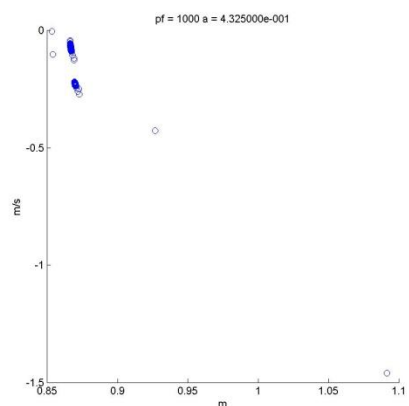
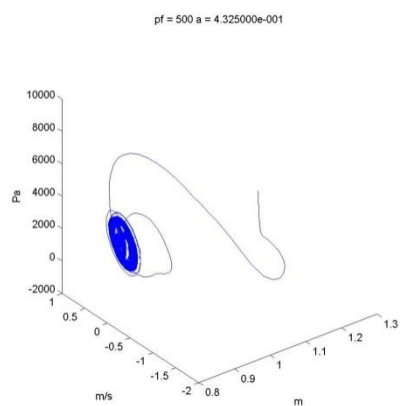
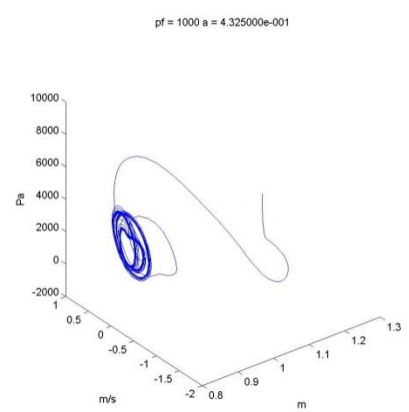
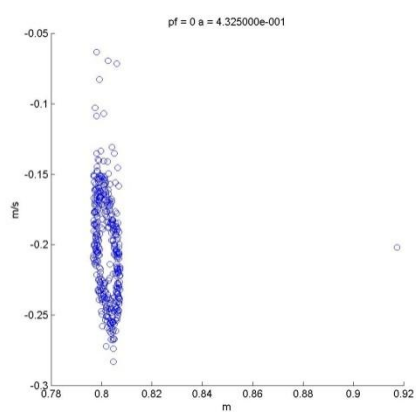
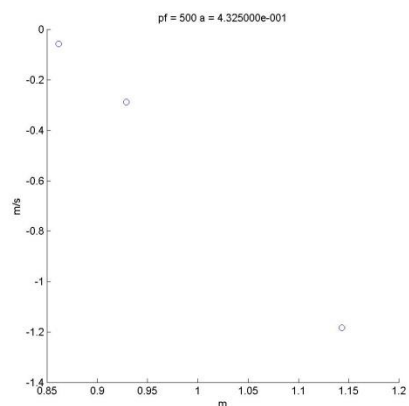
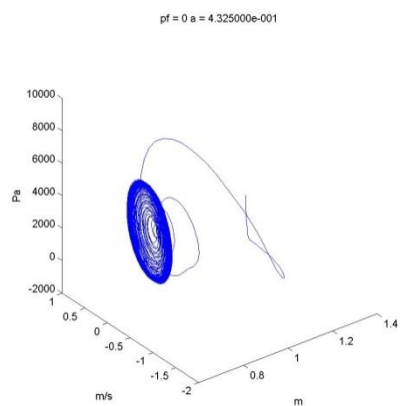


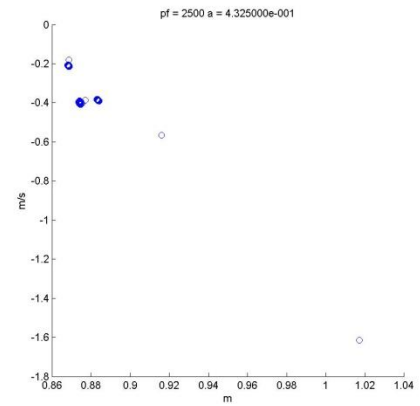
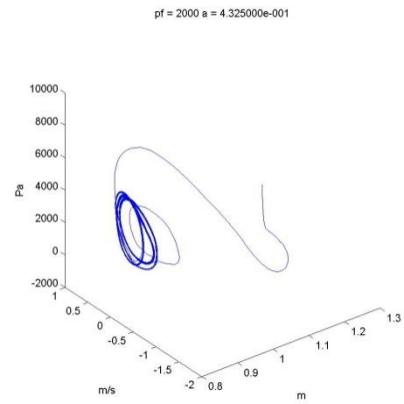
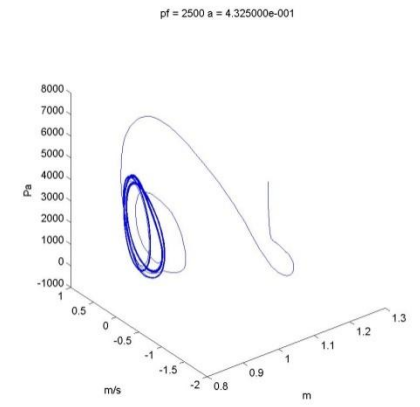
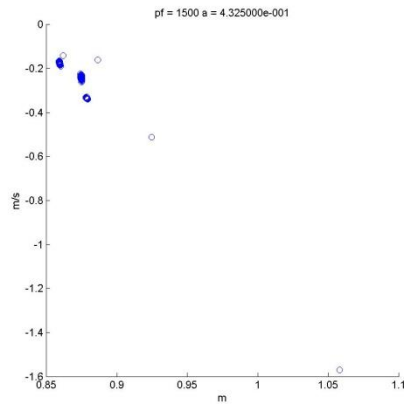
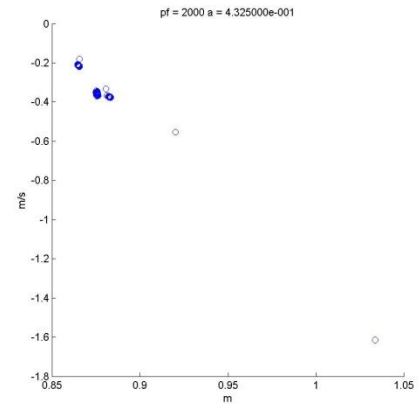
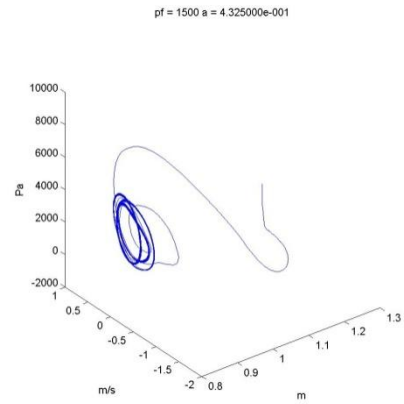












## VITA

Name: John Christian Bandas

Address: 917 John Paul Jones  
Temple, TX 76504

Email Address: jcbandas@gmail.com

Education: B.S., Ocean Engineering, Texas A&M University, 2009  
M.S., Ocean Engineering, Texas A&M University, 2012